

Nonparametric Bayesian Deconvolution of a Symmetric Unimodal Density

Ya Su

Department of Statistics, University of Kentucky, Lexington, KY 40536-0082, U.S.A.,
ya.su@uky.edu

Anirban Bhattacharya

Department of Statistics, Texas A&M University, College Station, TX 77843-3143, U.S.A.,
anirbanb@stat.tamu.edu

Yan Zhang and Nilanjan Chatterjee

Departments of Biostatistics and Oncology, Johns Hopkins University, Baltimore,
Maryland 21205, U.S.A., yzhan284@jhu.edu and nchatte2@jhu.edu

Raymond J. Carroll

Department of Statistics, Texas A&M University, College Station, TX 77843-3143, U.S.A.
and School of Mathematical and Physical Sciences, University of Technology Sydney,
Broadway NSW 2007, Australia, carroll@stat.tamu.edu

Abstract

We consider nonparametric measurement error density deconvolution subject to heteroscedastic measurement errors as well as symmetry about zero and shape constraints, in particular unimodality. The problem is motivated by applications where the observed data are estimated effect sizes from regressions on multiple factors, where the target is the distribution of the true effect sizes. We exploit the fact that any symmetric and unimodal density can be expressed as a mixture of symmetric uniform densities, and model the mixing density in a new way using a Dirichlet process location-mixture of Gamma distributions. We do the computations within a Bayesian context, describe a simple scalable implementation that is linear in the sample size, and show that the estimate of the unknown target density is consistent. Within our application context of regression effect sizes, the target density is likely to have a large probability near zero (the near null effects) coupled with a heavy-tailed distribution (the actual effects). Simulations show that unlike standard deconvolution methods, our Constrained Bayesian Deconvolution method does a much better job of reconstruction of the target density. Applications to a genome-wise association study (GWAS) and microarray data reveal similar results.

Some Key Words: Bayesian methods; Deconvolution; Effect sizes; Shape constraints

Short title: Deconvolution

1 Introduction

In important applied problems, one of which we discuss in Section 6 and the other in the **Supplementary Material**, data come from a one-dimensional classical measurement error model $W = X + U$, where the true density of X , $f_0(\cdot)$, is assumed to be unimodal and symmetric. We assume the error has density $\psi_\sigma(\cdot)$ with mean zero and a scale parameter σ , details can be found in the main text, whence the density of W , denoted p_0 , is the convolution of $f_0(\cdot)$ and $\psi_\sigma(\cdot)$. Given observations W_1, \dots, W_n , our interest lies in estimating the distribution of X under the given constraints. As part of our applications, we additionally consider the case where the scales of U_1, \dots, U_n are heteroscedastic, and denoted as $\sigma_1, \dots, \sigma_n$.

One of our motivations arises from genome-wide association studies (GWAS) containing a vast number of single nucleotide polymorphisms (SNPs) along with a response for a relatively small number of individuals, where the marginal effect sizes for the SNPs association with the response are of interest. Let W_i denote the estimated marginal effect size of the i th SNP obtained from a regression of the response on the i th centered and standardized SNP. It can be shown (see Section 6.2 for more details) that the true effect size for the i th SNP, X_i , can be related to W_i through $W_i = X_i + U_i$, with the U_i being approximately normally distributed, but heteroscedastic.

If we treat the true effect sizes X_i as random effects, the sampling distribution of X_i has two key features. First, it makes sense that the effect sizes will be symmetric about zero and unimodal, and not biased towards being marginally skew. This is the case in our two data applications, where the observed data have almost zero skewness and are unimodal. Second, in practice, we expect that most of the predictors have very small association with the response, with a handful possibly being practically significant. This suggests the density should have a sharp peak near zero while possibly being heavy-tailed; for an example of a density satisfying the two features above, see the blue solid curve in Figure 5. The primary challenge then lies in characterizing the density of X while properly capturing its expected shape.

There is a rich literature on density estimation in the measurement error context when

the measurement error is homoscedastic (Carroll and Hall, 1988; Fan, 1991; Stefanski and Carroll, 1990), among many others. Delaigle and Meister (2008) introduced a deconvoluting kernel technique for the heteroscedastic measurement error case; see also Sarkar et al. (2014) for a Bayesian approach. However, none of the existing approaches are designed to fulfill the specific constraints in our case. As a result, we are only able to compare our proposed approach with the general nonparametric kernel deconvolution estimator (Delaigle and Meister, 2008) in our simulations and real data examples.

In situations without any measurement error, there is some literature on modeling symmetric and unimodal densities. West (1987) studied scale-mixtures of Normals which notably includes the student- t and Laplace families. However, this approach is not fully flexible as there exist symmetric and unimodal densities for which the underlying mixing functions are not distributions (Chu, 1973). There are also methods based on Bernstein polynomial basis function where the shape constraints are preserved under constraints on the coefficients of the basis functions, e.g. Turnbull and Ghosh (2014). The disadvantages of using Bernstein polynomial bases are two fold. First, the distribution functions it can characterize exclude those whose support is $(-\infty, \infty)$. Second, the asymptotics of such shape constrained estimators are not well-studied in the literature even without the measurement error.

In this article, we propose a Bayesian approach for unimodal and symmetric density estimation in the measurement error context. The proposed method is easily adapted to a heteroscedastic error model, as we will exhibit. A key ingredient of the methodology is a representation theorem for symmetric and unimodal densities dating back at least to Feller (1971), where it was proved that any unimodal and symmetric density function can be represented by a mixture of uniform distributions. Brunner and Lo (1989) adopted this approach and modeled the mixing distribution via a Dirichlet process, which does not yield smooth densities owing to the almost sure discreteness of the Dirichlet process. To yield a smooth density, we model the mixing distribution using a Dirichlet mixture of Gamma distributions, which has large support on the space of smooth densities, and is amenable to scalable posterior computation via an efficient Gibbs sampler we develop here.

We provide large-sample theoretical support to the proposed methodology by showing posterior consistency for the observed density and the latent density. For the observed

density of W , we borrow results from recent work (Bochkina and Rousseau, 2017) where posterior convergence rates for estimating a density on the positive half-line were established using Dirichlet location-mixtures of Gamma distributions. Their setup nicely serves as a component in our hierarchical model for the density of W . While appreciating the value of their theory, the difficulty due to the hierarchical model we develop and the intrinsic deconvolution problem has not been discussed before and is highlighted in our current work.

We derive a posterior consistency result for the unobserved density of X under a Wasserstein metric. The Wasserstein metric has its origins in the theory of optimal transportation (Villani, 2008) and has recently been found suitable for studying convergence of mixing measures in deconvolution problems (Gao and van der Vaart, 2016; Nguyen, 2013; Scricciolo, 2018). These papers consider a Dirichlet process mixture type of model where the mixing distribution is discrete and needs to satisfy some conditions, see Section 3.3 for a discussion on their conditions. A key ingredient of our theory is the development of a new inversion inequality which relates the convergence of the observed/mixture density to that of the unobserved/mixing density. The idea of using inversion inequalities in the Bayes literature is fairly new, with only a few instances of such results, e.g., Nguyen (2013), Scricciolo (2018). However, existing inequalities can not be applied directly to our case, necessitating a new inversion inequality to fit our needs.

Section 2 gives the Bayesian model leading to our methodology, while Section 3 states asymptotic results. Section 4 describes our algorithm and Section 5 presents some of the many simulations we have conducted. Section 6 presents an analysis of a genome-wide association study, and shows that our methodology is able to capture the mixture distribution we expect to see in the data as described above. Section 7 gives concluding remarks. **Supplementary Material** includes additional data analysis of a microarray experiment.

2 Model Specification

Throughout our paper, $\psi(\cdot)$ denotes a symmetric unimodal density on the real line which specifies our family of error distributions. We further denote by $\psi_\sigma(\cdot)$ the corresponding scale family: $\psi_\sigma(t) = (1/\sigma)\psi(t/\sigma)$ for $\sigma > 0$. Finally, $\Psi_{\mu,\sigma}(\cdot)$ denotes the distribution function

with density (in t) given by $(1/\sigma)\psi\{(t - \mu)/\sigma\}$.

Since $W = X + U$, the true density $p_0(\cdot)$ of W has the form

$$p_0(w) = \int \psi_\sigma(w - x)f_0(x)dx, \quad (1)$$

where the true density of X , $f_0(\cdot)$, has a unimodal and symmetric shape. If f_0 is continuous with finite derivative $f_0'(x)$ for all x , then it is well-known (Feller, 1971) that there exists a density $g_0(\cdot) : \mathbb{R}^+ \rightarrow \mathbb{R}^+$, where $\mathbb{R}^+ = [0, \infty)$, such that

$$f_0(x) = \int (2\theta)^{-1}I_{(-\theta \leq x \leq \theta)}g_0(\theta)d\theta. \quad (2)$$

In other words, any symmetric and unimodal density is a mixture of symmetric uniforms. Given our motivating application, it is natural to assume in addition that $f_0(\cdot)$ is finite at zero, which ensures the finiteness of $p_0(\cdot)$. The finiteness of $f_0(0)$ can in turn be ensured by assuming that $g_0(0) = 0$. Our parameter space for $g_0(\cdot)$ thus consists of all densities on the positive half-line \mathbb{R}^+ satisfying $g_0(0) = 0$.

In the deconvolution literature, two types of error distributions, ordinary-smooth and super-smooth, are commonly studied. By definition, a density is ordinary-smooth or super-smooth if the tail of its Fourier transform decays to zero at polynomial rate or exponential rate, respectively. For our theoretical analysis and simulation studies, we pick one distribution from each class, namely the Normal and Laplace distributions. When presenting the theory we illustrate the Normal error case first, while the results for the Laplace error distribution are studied in a separate section. A similar strategy has been taken with the proofs. Furthermore in a more complicated situation when only the type (ordinary-smooth or super-smooth) is known, we point out the possibility of modeling the error distribution using mixtures of Normal/Laplace distributions prior; see Sarkar et al. (2017) for an instance of the former.

We build our Bayesian model in a hierarchical structure as the true densities, that is, the candidate densities $p(\cdot)$, $f(\cdot)$ and $g(\cdot)$ are defined in a similar way as in (1) and (2). In particular, given the representation (2), the problem of modeling $f(\cdot)$ equivalently reduces to creating a flexible model for $g(\cdot)$. Recall that $g(\cdot)$ is supported on \mathbb{R}^+ . We model $g(\cdot)$ using a Dirichlet process location-mixture of Gamma distributions, which has large support

(Bochkina and Rousseau, 2017) on densities supported on \mathbb{R}^+ , and is easy to implement in a Bayesian framework. Specifically, we reparameterize a Gamma density by its shape z and mean μ as parameter pairs. Denote $g_{z,z/\mu}$ to be a Gamma density with shape z and rate z/μ ; we use $\text{Ga}(z, z/\mu)$ to denote the corresponding probability distribution. We assume a Dirichlet process prior (Ferguson, 1973) on the distribution of μ and another prior Π_z on z . With these ingredients, our hierarchical Bayesian model is

$$\begin{aligned} W_i|X_i &\sim \Psi(X_i, \sigma); & X_i|\theta_i &\sim \text{Unif}(-\theta_i, \theta_i); & \theta_i|z, \mu &\sim \text{Ga}(z, z/\mu); \\ \mu|P_\mu &\sim P_\mu; & P_\mu|m, D &\sim \text{DP}(m, D); & z &\sim \Pi_z, \end{aligned}$$

where $\text{Unif}(\theta_1, \theta_2)$ is a Uniform distribution on the interval $[\theta_1, \theta_2]$ and $\text{DP}(m, D)$ denotes a Dirichlet process with concentration parameter m and base probability measure D . The hyperparameters are m and other possible parameters for specification of D and Π_z .

Using the stick-breaking representation (Sethuraman, 1994) for the Dirichlet process, the model-prior for $g(\cdot)$ can be represented as

$$\begin{aligned} g(x) &= \int \left\{ \sum_{h=1}^{\infty} \nu_h \text{Ga}(x | z, z/\mu_h) \right\} \Pi_z(dz), \\ \nu_h &= \nu_h^* \prod_{\ell < h} (1 - \nu_\ell^*), & \nu_\ell^* &\sim \text{Beta}(1, m), & \mu_h &\sim D, \end{aligned}$$

where $\text{Ga}(x | z, z/\mu_h)$ denotes the $\text{Ga}(z, z/\mu)$ density evaluated at x . For numerical computation, we use a finite Dirichlet approximation (Ishwaran and Zarepour, 2002) to the Dirichlet process in our simulations and data examples.

3 Theoretical Analysis

3.1 Goal and Background

In this section, we provide theoretical support to our method in terms of posterior consistency for the observed and latent densities. Specifically, we show that the posterior distribution for $p(\cdot)$ and $f(\cdot)$ increasingly concentrates on arbitrarily small neighborhoods of the true densities $p_0(\cdot)$ and $f_0(\cdot)$, respectively, as the sample size increases.

We follow the general procedures in Ghosal et al. (2000) of establishing posterior contraction theory and make substantial modifications to adapt to the hierarchical model considered

in this paper. We begin with a basic model with no measurement error and then build the theory towards its measurement error counterpart, allowing multiple layers of mixture in the latter case. Another novelty of the current approach is its ability to work with X having a continuous density with infinite support, as opposed to a discrete density with finite support considered in Nguyen (2013). This is achieved by a mixture model with a mixing distribution modelled by a Dirichlet Process mixture of Gamma distributions. We obtain some preliminary results on this layer from Bochkina and Rousseau (2017). An inversion inequality is derived that bridges our theory from $p(\cdot)$ to $f(\cdot)$.

We list some key definitions and notation in this section. Let μ and ν be two probability measures defined on a metric space with metric d . If μ and ν both have finite p th moments, the p th Wasserstein distance (Villani, 2008), denoted $W_p(\mu, \nu)$, is defined as $W_p^p(\mu, \nu) = \inf_{\phi \in \Gamma(\mu, \nu)} \int d^p(x, y) d\phi(x, y)$, where $\Gamma(\mu, \nu)$ represents the collection of all joint measures with marginal measures μ and ν . We consider the metric space \mathbb{R} with the Euclidean distance $d(x, y) = |x - y|$. For any two densities $p_1(\cdot)$ and $p_2(\cdot)$ on \mathbb{R} , $W_p(p_1, p_2)$ is the same as $W_p(P_1, P_2)$ where P_1 and P_2 are the cumulative distribution functions corresponding to $p_1(\cdot)$ and $p_2(\cdot)$, respectively. Another distance metric between two probability densities $p_1(\cdot)$ and $p_2(\cdot)$ is the Hellinger distance, $h(p_1, p_2) = (1/2) \int \{p_1(x)^{1/2} - p_2(x)^{1/2}\}^2 dx$. The Hellinger distance is widely used in the Bayesian asymptotics literature for quantifying posterior consistency or convergence of densities. The notation $\Pi_n(A_n | W_1, \dots, W_n)$ stands for a posterior probability of an event A_n given the observations W_1, \dots, W_n .

To make notation simpler, from now on, we assign an overall symbol P_0 for probability or expectation under the true distribution of the corresponding variable, e.g., $P_0(W > s)$ or $P_0(X > s)$ mean the probability that $W > s$ or $X > s$ under the true p_0 or f_0 respectively. Also, $a_n \lesssim b_n$ ($a_n \gtrsim b_n$) means that there exists a positive constant C such that $a_n/b_n \leq C$ ($a_n/b_n \geq C$) for all n . In addition, $a_n \asymp b_n$ if and only if $a_n \lesssim b_n$ and $a_n \gtrsim b_n$, $a \vee b = \max(a, b)$, $a \wedge b = \min(a, b)$. Finally, $\lceil a \rceil$ denotes the smallest integer that is greater than or equal to a .

3.2 Posterior Consistency for the Observed Density

This section gives a theorem on the posterior convergence rate for $p(\cdot)$. Our conditions are mainly at the layer of $g(\cdot)$, which is modelled as a Dirichlet location-mixture of Gamma distributions. We will give the conditions followed by some interpretations on these conditions and then state the theorem.

Condition 1. We adopt a function space for $g_0(\cdot)$, $\mathcal{M}\{L(\cdot), \varpi, C_0, C_1, e, \Delta\}$, which contains a set of density functions $q : \mathbb{R}^+ \rightarrow [0, \infty)$ which satisfy that there exists $L(\cdot) > 0, \varpi \geq 0, C_0 > 0, C_1 > 0, e > 0$ and Δ that for all $\theta \in \mathbb{R}^+, \phi > -\theta$ and $|\phi| \leq \Delta$,

$$|q(\theta + \phi) - q(\theta)| \leq L(\theta)|\phi|(1 + |\phi|^\varpi); \quad q(\theta) \leq C_0;$$

$$\int_0^\infty \{(1 + \theta^\varpi)\theta L(\theta)/q(\theta)\}^2 q(\theta) d\theta \leq C_1.$$

Condition 2. For some $\rho_1 > 2$, $\int_x^\infty \theta^4 g_0(\theta) d\theta \leq C(1 + x)^{-\rho_1 + 2}$.

Condition 3. (i) The prior on P_μ is $\text{DP}(m, D)$, where D has a positive and continuous density $d(\cdot)$ on \mathbb{R}^+ satisfying that for some $0 < a'_0 \leq a_0$ and $0 < a'_1 \leq a_1$,

$$\exp(-x^{-a_0}) \lesssim d(x) \lesssim \exp(-x^{-a'_0}) \text{ as } x \rightarrow 0;$$

$$\exp(-x^{a_1}) \lesssim d(x) \lesssim \exp(-x^{a'_1}), \text{ as } x \rightarrow \infty.$$

(ii) The prior on z , Π_z , has support $(1, \infty)$. For constants $c \geq c' > 0, c_0 > 0$ and $\rho_z \geq 0$,

$$\Pi_z([x, 2x]) \gtrsim \exp\{-c\sqrt{x}(\log x)^{\rho_z}\}, \quad \Pi_z([x, \infty)) \lesssim \exp\{-c'\sqrt{x}(\log x)^{\rho_z}\} \text{ as } x \rightarrow \infty,$$

$$\Pi_z((1, x]) \lesssim (x - 1)^{c_0} \text{ as } x \rightarrow 1.$$

For notational simplicity, we drop the arguments and only use \mathcal{M} to denote the space of densities in Condition 1. Similar function spaces with additional smoothness assumptions have been used by Bochkina and Rousseau (2017); we do not make such smoothness assumptions here. The conditions are typical in the literature on Bayesian density estimation. A density satisfying Condition 1 and Condition 2 can be well approximated by a mixture of Gamma distributions which facilitates finding a KL divergence neighbourhood around the true observed density $p_0(\cdot)$. When the error distribution is Laplace, Condition 2 is slightly

relaxed, see Condition 2' below. Condition 3 (i) is on the base measure of Dirichlet process and agrees with that in Shen et al. (2013) except that the support is on $(0, \infty)$ instead of $(-\infty, \infty)$. Condition 3 mainly controls the prior thickness of the sieve space upon which the inversion inequality in Section 3.3 can be derived. Bochkina and Rousseau (2017) showed Condition 1 is satisfied by Weibull, folded Student-t and Frechet-type densities. Condition 3 (ii) holds, for example, if \sqrt{z} has a Gamma prior.

Clearly, the prior is hierarchical, Condition 1 and Condition 2 are imposed on $g_0(\cdot)$ which is free of shape constraints except that it is a density on the positive half line. It is generally difficult to do the other way around, that is, impose conditions on $f_0(\cdot)$ and identify its corresponding properties on $g_0(\cdot)$. However, we can verify these conditions under some special cases. When $f_0(\cdot)$ is a Normal density with mean zero and standard deviation σ , $g_0(\theta) = C(\theta/\sigma)^2 \exp\{-(\theta/\sigma)^2\}$ which belongs to a Weibull family of distributions. Therefore Condition 1 is met. Condition 2 holds for arbitrarily large ρ_1 . When $f_0(\cdot)$ is a t-distribution with degrees of freedom ν , $g_0(\theta) = C\theta^2(1 + \theta^2)^{-(\nu+3)/2}$ which is an Inverse Beta distribution. Condition 1 can be verified by similar arguments in Bochkina and Rousseau (2017) for a folded Student-t density since only the tail behavior of its derivatives matters. Condition 2 holds when $\nu > 4$ with $\rho_1 = \nu - 2$.

Theorem 1. Fix $\epsilon > 0$. Under Conditions 1–3, for any $M > 0$ large enough,

$$\lim_{n \rightarrow \infty} \Pi_n(\{p : h(p, p_0) > M\epsilon\} | W_1, \dots, W_n) = 0 \text{ almost surely.}$$

Proof. To prove Theorem 1, we shall exhibit a sequence $\epsilon_n \rightarrow 0$ such that

$$\lim_{n \rightarrow \infty} \Pi_n(\{p : h(p, p_0) > M\epsilon_n\} | W_1, \dots, W_n) = 0 \text{ almost surely.}$$

To prove the assertion in the above display, it follows from Ghosal et al. (2000) that the desired result holds as long as there exists a sequence of compact subsets $\{\mathcal{F}_n\}$ in the space where $p(\cdot)$ resides and a sequence $\{\tilde{\epsilon}_n\}$ with $\tilde{\epsilon}_n \leq \epsilon_n$ and $\lim_{n \rightarrow \infty} n\tilde{\epsilon}_n^2 = \infty$ such that

$$\log N(\epsilon_n, \mathcal{F}_n, h) \leq c_1 n \epsilon_n^2; \tag{3}$$

$$\Pi(\mathcal{F}_n^c) \leq c_3 \exp\{-(c_2 + 4)n\tilde{\epsilon}_n^2\}; \tag{4}$$

$$\Pi\{p : P_0 \log(p_0/p) \leq A\tilde{\epsilon}_n^2, P_0\{\log(p_0/p)\}^2 \leq A\tilde{\epsilon}_n^2 \log n\} \geq \exp(-c_2 n \tilde{\epsilon}_n^2), \tag{5}$$

for some positive constants c_1, c_2, c_3, A , and $N(\epsilon_n, \mathcal{F}_n, h)$ is the ϵ_n -covering number of \mathcal{F}_n relative to the Hellinger distance. Equations (3) and (4) are entropy and prior mass conditions on the sieve space and (5) is referred to as the prior concentration condition. Equation (5) is a slight variation compared to the original prior concentration condition in Ghosal et al. (2000); see Bochkina and Rousseau (2017).

In Appendix A.1, the details for deriving equations (3), (4) and (5) are provided for $\tilde{\epsilon}_n^2 = \epsilon_n^2 \asymp n^{-2/(2B+3)}(\log n)^{(2B+2)/(2B+3)}$ and an appropriate sieve space \mathcal{F}_n . The constant B in ϵ_n is determined by the constants ρ_1, a_0 and a_1 in Condition 2 and 3 (i). \square

3.3 Posterior Consistency for the Latent Density

We now establish that the posterior distribution for the latent density $f(\cdot)$ increasingly concentrates around the true density $f_0(\cdot)$. To show such a result, we build an inversion inequality which harnesses the consistency of the observed density $p(\cdot)$ derived above to prove consistency for the latent density $f(\cdot)$. A few previous instances of inversion inequalities can be found in the recent literature. Theorem 2 of Nguyen (2013) relates the Wasserstein distance between the mixing distributions with the total variation of the mixture density, but it requires the mixing distribution to reside on a finite support or have bounded $s > 2$ moment. Scricciolo (2018) makes use of an inversion inequality to establish the convergence rate of the Bayes estimator for the mixing density; one of the key requirements on the mixing distribution is that it has a bounded moment generating function on some interval containing $[-1, 1]$. However, there does not exist an inversion inequality that can be directly applied to our problem, where the mixing density $f(\cdot)$ has unbounded support and there is no way to bound the moment generating function on any interval containing $[-1, 1]$ for all $f(\cdot)$ in a sieve space. In Appendix A.2, we prove the next Lemma that relates the convergence of $f(\cdot)$ to $f_0(\cdot)$ under the Wasserstein metric, $W_2(f, f_0)$, and the L_1 distance between $p(\cdot)$ and $p_0(\cdot)$.

Lemma 1. On the sieve \mathcal{F}_n in Theorem 1, when ρ_1 and a'_1 (see Condition 2 and Condition 3) are large enough,

$$W_2^2(f, f_0) \lesssim \{-\log(\|p - p_0\|_1)\}^{-1}.$$

Remark 1. For any two densities p_1, p_2 , $\|p_1 - p_2\|_1/2 \leq h(p_1, p_2) \leq \|p_1 - p_2\|_1^{1/2}$. The conclusion of Lemma 1 can be equivalently stated as $W_2^2(f, f_0) \lesssim [-\log\{h(p, p_0)\}]^{-1}$.

Theorem 2. Fix $\varepsilon > 0$. Under the Conditions in Theorem 1 and Lemma 1, for any $M > 0$ large enough, $\lim_{n \rightarrow \infty} \Pi_n[f : W_2(f, f_0) > M\varepsilon | W_1, \dots, W_n] = 0$ almost surely.

Proof. Theorem 2 follows from Theorem 1 and Lemma 1. □

Remark 2. Theorem 2 states that the posterior consistency of $f(\cdot)$ in the W_2 metric as a result of the presence of the W_2 metric in the inversion inequality in Lemma 1. In fact, the proof of Lemma 1 can be extended to W_k for any $k \geq 1$, which in turn would imply posterior consistency in any W_k metric. To the best of our knowledge, technical difficulties exist in order to derive Lemma 1 for the L_1 metric between $f(\cdot)$ and $f_0(\cdot)$. The difficulties lie in finding a *uniform* upper bound for the L_1 distance between functions in the sieve space and its convolution with the mollifier. Whereas if Wasserstein distance (of order 2) is in use, such an upper bound is simply the second moment of the mollifier. This is probably the hurdle if one wants to establish posterior contraction theory in L_1 distance for the mixing density without restricting oneself on special cases of the mixing density.

3.4 Theory when the error has a Laplace distribution

All theorems and Lemmas in Section 3.2 and Section 3.3 can be derived when the measurement error has a Laplace distribution under a relaxation of Condition 2. We state the condition and theorems whenever changes are met.

Condition 2'. For some $\rho_1 > 0$, $\int_x^\infty \theta^2 g_0(\theta) d\theta \leq C(1+x)^{-\rho_1}$.

It can be inferred that Condition 2' holds for $\rho_1 > 2$ assuming Condition 2. The statement in Theorem 1 holds under Condition 1, 2' and 3.

Lemma 2. On the sieve \mathcal{F}_n in Theorem 1, when ρ_1 and a'_1 , see Condition 2', and 3 (i) are large enough, there exists a $\nu > 0$ depending on ρ_1 and a'_1 such that

$$W_2^2(f, f_0) \lesssim \|p - p_0\|_1^\nu.$$

Theorem 1 and Lemma 2 together imply that Theorem 2 holds.

The proofs are along the lines of their correspondence to the Normal error case. They are in Appendix A.1 with only the differences presented.

4 Algorithm

To ease computational complexity, we follow standard practice by approximating the Dirichlet process mixture prior with a finite mixture of Gamma distributions with K components where K is large, with a specific Dirichlet prior on the mixture probabilities (Ishwaran and Zarepour, 2002). It is trivial to implement our procedure for the infinite mixture using the slice sampler of Kalli et al. (2011); however we prefer the finite Dirichlet due to its substantially better mixing behavior for our multi-layered hierarchical model. Our theoretical results in Section 3 were developed for the Dirichlet location-mixture of Gamma priors on $g(\cdot)$, where only the mean parameter is mixed over. For flexibility, we adopt a mixture on both the shape and rate parameters for our numerical implementation. The conditions on the priors for these parameters become less stringent because the number of such parameters is finite. We select these priors among some popular choices. Specifically, our hierarchical Bayes model for subsequent implementations is as follows. Let i denote the index for subject, and k be the index for the k th component, for all $i = 1, \dots, n$, $k = 1, \dots, K$. Let $t > 1$ denote a fixed constant. Then,

$$\begin{aligned} (W_i|X_i) &\sim \Psi(X_i, \sigma_i); \quad (X_i|\theta_i) \sim \text{Unif}(-\theta_i, \theta_i); \quad (\theta_i|Z_i = k, \alpha_k, \beta_k) \sim \text{Ga}(\alpha_k, \beta_k); \\ P(Z_i = k|p_1, \dots, p_K) &= p_k; \quad (\alpha_k|\lambda, t) \sim \text{Expon}(\lambda; t, \infty); \quad (\beta_k|\Xi_1, \Xi_2) \sim \text{Ga}(\Xi_1, \Xi_2); \\ (p_1, \dots, p_K) &\sim \text{Dirichlet}(m/K, \dots, m/K), \end{aligned}$$

where $\text{Dirichlet}(\gamma_1, \dots, \gamma_K)$ denotes a Dirichlet distribution with parameters $\gamma_1, \dots, \gamma_K$, $\text{Expon}(\lambda; \ell, u)$ denotes an exponential distribution with parameter λ truncated at (ℓ, u) . The paragraph above Theorem 1 points out the reason for truncating α_k . The set of hyperparameters is $(\lambda, t, \Xi_1, \Xi_2, K, m)$.

Denote the set of all variables and hyperparameters given above as

$$\Omega = (\{W_i\}_{i=1}^n; \{X_i\}_{i=1}^n; \{\theta_i\}_{i=1}^n; \{Z_k\}_{k=1}^K; \{\alpha_k\}_{k=1}^K; \{\beta_k\}_{k=1}^K; \{p_k\}_{k=1}^K; \lambda, t, \Xi_1, \Xi_2, K, m).$$

For ease of notation, let $\boldsymbol{\Omega}_{-\zeta}$ be all variables in $\boldsymbol{\Omega}$ but excluding ζ . For $k = 1, \dots, K$, let $r_k = \sum_i I_{(Z_i=k)}$ be the total number of individuals that fall into group k and $s_k = \sum_i \theta_i I_{(Z_i=k)}$ be the summation of the θ_i from the k th group. To sample from the posterior distribution of $\boldsymbol{\Omega}$, we use a Gibbs sampler for all parameters other than the α_k , combined with a Metropolis-Hastings within Gibbs for the α_k . The posterior full-conditional distributions are

$$\begin{aligned}
(X_i | \boldsymbol{\Omega}_{-X_i}) &\sim \Psi(W_i, \sigma_i; -\theta_i, \theta_i); \\
(\theta_i | \boldsymbol{\Omega}_{-\theta_i}) &\sim \text{Ga}(\alpha_{Z_i} - 1, \beta_{Z_i}; |X_i|, \infty); \\
P(Z_i = k | \boldsymbol{\Omega}_{-Z_i}) &\propto \Gamma(\alpha_k)^{-1} p_k(\beta_k \theta_i)^{\alpha_k} \exp(-\beta_k \theta_i); \\
(p_1, \dots, p_K | \boldsymbol{\Omega}_{-\{p_1, \dots, p_K\}}) &\sim \text{Dirichlet}(m/K + r_1, \dots, m/K + r_K); \\
(\beta_k | \boldsymbol{\Omega}_{-\beta_k}) &\sim \text{Ga}(\Xi_1 + \alpha_k r_k, \Xi_2 + s_k); \\
(\alpha_k | \boldsymbol{\Omega}_{-\alpha_k}) &\propto \Gamma(\alpha_k)^{-r_k} \exp\{-\alpha_k(\lambda - r_k \log \beta_k - \sum_i \log(\theta_i) I_{(Z_i=k)})\}.
\end{aligned}$$

The symbol $\Psi(\mu, \sigma; \ell, u)$ denotes the distribution $\Psi(\mu, \sigma)$ truncated at (ℓ, u) . Meanwhile $\text{Ga}(\alpha, \beta; \ell, u)$ corresponds to a Gamma distribution with parameters (α, β) truncated at (ℓ, u) . Since the posterior distribution of α_k does not belong to a standard family, we implement a Metropolis-Hastings algorithm within the Gibbs sampler to update the α_k . We use a Gamma proposal distribution; specifically, $\tilde{\alpha}_k \sim \text{Ga}(2, 2/\alpha_k; t, \infty)$, and we accept the proposed $\tilde{\alpha}_k$ or keep the original α_k according to the general Metropolis-Hastings rule. The proposal distribution is truncated to reflect the prior assumption on α_k .

For all of our simulations presented, we treat the error variances σ_i^2 for all U_i as known: this is reasonable in our examples, and often used in the standard deconvolution theory. The default selected values for hyperparameters are $\lambda = 2, t = 2.5, \Xi_1 = 1, \Xi_2 = 4, K = 8, m = 20$. Sensitivity analysis showed little sensitivity to different choices of the hyperparameters. The marginal density for X , our estimator, is computed as the average value of the marginal density at each MCMC iteration. We name the method as Bayes density deconvolution with shape constraint estimator (Constrained Bayes Deconvolution).

Our Constrained Bayes Deconvolution method is easily seen to be scalable in that it is linear in the sample size, and indeed in Section 6.2 it is show to be able to handle sample size of nearly 10^6 : it is written in R with use of the package RCPP.

5 Simulations

5.1 Overview

We conducted simulations for two distinctly different problems. In the first, the target density for X has a standard t-distribution with 5 degrees of freedom. In the second, related to our examples, X has a density that is a mixture of (a) t random variables with 5 degrees of freedom; and (b) values with mean zero and very small variability. In addition, for each of (a) and (b), we consider the case of homoscedastic and heteroscedastic measurement errors generated from either the Normal or the Laplace distributions.

Case (b) is the important one for us given the type of data we want to analyze, while Case (a) is simply meant to show that we are competitive with the standard method, namely the kernel density deconvolution estimator, in standard problems. The kernel estimator has two versions depending on whether the measurement errors are homoscedastic or heteroscedastic. The plug-in bandwidth, which minimizes the asymptotic mean integrated squared error, is chosen for this estimator in comparison with our method, see Delaigle and Meister (2008). The R package, `deconvolve`, published on Github implements the kernel density deconvolution estimator.

In each design of the simulation we generated data with sample sizes $n = 1,000, 5,000$, each repeated with 100 simulated data sets.

We compute posterior samples of the density across the MCMC steps and the estimated density is obtained as the mean of these posterior samples. The estimated densities and the true density are compared via the square root of the integrated squared error (ISE), the integrated absolute error (IAE) and the Wasserstein distance (W_2) for each simulated data set. An overall summary is given in Section 5.4.

5.2 When X has a t-distribution With 5 Degrees of Freedom

We generated observations by $W_i = X_i + U_i$, X_i has a t distribution with 5 degrees of freedom. In the case of homoscedastic error, the variance of U is equal to the variance of X , specifically, $\text{Var}(U_i) = 1.66$. In the heteroscedastic case, $\text{Var}(U_i) = (1 + X_i/4)^2$, with

the variance of X being 1.5 times the mean of $\text{Var}(U_i)$. In all cases, the observations are subject to substantial measurement error. The estimated densities are displayed in Figure 1 – Figure 4. The numerical comparisons for our Constrained Bayes Deconvolution method and the Kernel method are given in Table 3 – Table 4.

5.3 When X has a Tight Peak Around Zero

The setting in this section is designed for cases when the distribution of X has a large probability clustered near zero, as we expect in our examples. One way to do this is through a mixture structure, assuming that the density of X has a component that is tightly concentrated at zero and another component from a standard density. We implement a mixing of a $\text{Normal}(0, \sigma_{00}^2)$ for the first component and a t -distribution with 5 degrees of freedom for the second component, with mixing probabilities 0.8 and 0.2 respectively. We choose the small value $\sigma_{00} = 0.2$ so that the mixing density has a very sharp peak around zero. For $\sigma_{00} = 0.2$ $\text{var}(X) = 0.37$.

In this case, when the true density puts a high concentration around zero, in addition to the usual global metrics IAE, ISE and W_2 , it is interesting to study how well an estimated density can capture the probability greater than, in absolute value, 3 times the standard deviation of the “tight peak” component. With a small abuse of notation, in the following, “Exceedance” is defined as the absolute difference between the exceedance probability under the estimated density and that under the true density.

In the case of homoscedastic error, $\text{Var}(U_i) = 0.36$, such that the variance of U is equal to the variance of X . We implement the heteroscedastic case by adjusting an appropriate form for $\text{Var}(U_i)$ in Section 5.2 such that the mean of $\text{Var}(U_i)$ is more than the variance of X , specifically, $\text{Var}(U_i) = (0.75 + X_i/4)^2$. Again in all cases, the observations are subject to substantial measurement error. The estimated densities are displayed in Figure 5 – Figure 8. The numerical comparisons for our Constrained Bayes Deconvolution method and the Kernel method are given in Table 5 – Table 6.

5.4 Conclusions from the Simulations

For both the simulations in Section 5.2 and Section 5.3, with either homoscedastic or heteroscedastic error, we observe that under the global metrics ISE and IAE, large gains in efficiency are achieved with our Constrained Bayes Deconvolution estimator over the deconvoluting kernel estimator across all choices of sample size. Also, from the figures and tables of Section 5.3, with either homoscedastic or heteroscedastic error, the Constrained Bayes Deconvolution estimator performs much better in capturing the peak as well as the tail behavior, from both a visual check and the Exceedance metric. Lastly, the kernel deconvolution estimator gives a biased peak for our sample sizes when the errors are heteroscedastic.

6 Genome Wide Association Applications

6.1 Background

In this section, we describe the results of a genome-wide association study (GWAS) that is particularly appropriate. In the **Supplementary Material**, we also describe results from a microarray experiment, which reaches similar conclusions.

6.2 Height data

Our data come from a genome-wide association study for height (Allen et al., 2010). The study data we have involves 133,653 individuals, and each individual in our data set has 941,389 SNPs that were measured. The goal of the study was to understand which SNPs were related to height, either positively or negatively. Because of the relative rareness of traits that affect height, the simulation of Section 5.3 is particularly relevant.

The data we have access to are regression coefficients of standardized heights, Y_k say, on standardized SNPs for SNP i , Z_{ik} say, and are thus estimated effect sizes. If we regress the Y_k on the Z_{ik} , it is easy to see that if the true effect size is $X_i = \beta_i$, the estimated effect size is $W_i = \hat{\beta}_i$, which, because of the sample size involved, is approximately normally distributed with mean β_i and measurement error $U_i = \text{Normal}(0, \sigma_i^2)$, where $\sigma_i^2 = \sigma_{i\epsilon}^2/n$, where n is the

sample size and $\sigma_{i\epsilon}^2$ is the regression variance of the Y_k on the Z_{ik} . Clearly, because of the sample size and the division by n , $\text{var}(U_i) = \sigma_i^2$ is well-estimated and thus essentially known, but heteroscedastic.

For our Constrained Bayes Deconvolution estimator, we run 5000 MCMC iterations using the same hyperparameters used in the simulation section. There was a difficulty with the deconvoluting kernel density estimator, because its current implementation is exceedingly slow in terms of computation and resulted in a memory issue on a Linux machine with Intel(R) Xeon(R) CPU E5-2690 0 @ 2.90GHz. As a result, we subsampled 1% of the SNPs (by taking every 100th SNP) to obtain results for this estimator, although such subsampling was unnecessary for our efficient implementation of the Constrained Bayes Deconvolution estimator. We have confirmed that our Constrained Bayes Deconvolution estimator gave very similar results for both the full data and the subsampled data. We also ran the R package Kern Smooth to obtain the naive Kernel density estimator that ignores measurement error: as expected, our Constrained Bayes Deconvolution estimator dominated it as well for both the full and subsampled data.

The resulting density estimators are shown in Figure 9. Among the three, our Constrained Bayes Deconvolution method yields a density that has a much sharper peak. This is expected, as in the simulation of Section 5.3, because regular kernel methods, deconvolved or not, cannot handle well this type of very non-standard, but practically important, density.

In addition to the graphical comparison, quantitative comparisons were also made. We compute the estimated probability of the effect size in absolute value being greater than some choices of minimum effect size, displayed in Table 1 and Figure 10. As mentioned above, the effect sizes for all SNPs are chosen for our Constrained Bayes Deconvolution and naive Kernel estimators while that of every 100th SNP are selected for the Kernel deconvolution estimator.

A scientific question in GWAS is to predict the number of significant SNPs for a given sample size, i.e., the number of individuals. Current scientific discoveries are based on the significance of p-values (with a Bonferroni significance level $\alpha = 5 \times 10^{-8}$) for individual SNPs followed by a “LD clumping” step which selects independent SNPs using their linkage disequilibrium. In recently published GWAS studies of height, Allen et al. (2010), Wood

Estimator	Minimum effect size						
	0.002	0.0025	0.003	0.0035	0.004	0.0045	0.005
Constrained Bayes	0.253	0.175	0.104	0.067	0.040	0.021	0.007
Kernel	0.426	0.346	0.286	0.226	0.191	0.159	0.130
Naive Kernel	0.561	0.466	0.382	0.310	0.248	0.196	0.133

Table 1: Comparison of estimated probability of effect sizes associated with height that the absolute value of effect sizes is greater than the given minimum effect size under our Constrained Bayes Deconvolution method (Constrained Bayes), the deconvoluting kernel density estimator (Kernel) and the naive ordinary kernel density estimator (Naive Kernel) for the GIANT Height effect sizes.

et al. (2014), and Yengo et al. (2018), the number of individuals increased from 133K, 253K, to 700K, leading to 180, 697, and 3290 significant discoveries using the described method or more complicated methods regarding the joint SNP effects.

We now briefly discuss the relevance of our density estimation procedure towards such sample size calculations; additional details are deferred to Section S.1.2 of **Supplementary Material**. Suppose $\widehat{\beta} \mid \beta \sim N(\beta, \sigma^2/n)$, where $\widehat{\beta}$ denotes an observed effect size, β denotes the corresponding true effect size with density f , and the error variance σ^2 is displayed as a constant here for notational simplicity. A standard approach (Chatterjee et al., 2013) for predicting the number of effect sizes achieving genome-wide significance α at sample size n is provided by the projection formula, $n \times \Pr(\sigma^{-1}\sqrt{n}|\widehat{\beta}| > z_{\alpha/2}) = n \int \text{pow}_{\sigma,\alpha}(\beta) f(\beta) d\beta$, where $\text{pow}_{\sigma,\alpha}(\beta) = 1 - \Phi(z_{\alpha/2} - \sqrt{n}\sigma^{-1}\beta) + \Phi(-z_{\alpha/2} - \sqrt{n}\sigma^{-1}\beta)$. Here $\Phi(\cdot)$ and $z_{\alpha/2}$ denote the cumulative distribution function and the $(1 - \alpha/2)$ th quantile of a standard normal random variable.

We can obtain point and interval estimates for the quantity $\int \text{pow}_{\sigma,\alpha}(\beta) f(\beta) d\beta$ from our MCMC output. A Monte Carlo integration is performed to approximate the projection formula using the posterior samples of β , leading to the desired point prediction. We can further quantify the posterior variability of the predicted number by repeating the calculation on slices dispersed over a MCMC chain. Since scientists are generally interested in the number of independent SNPs that are discovered, we first selected a subset of independent SNPs based on the linkage disequilibrium between the SNPs before estimating the density

of X using our procedure. More details about the above procedures can be found in Section S.1.1.2 of **Supplementary Material**.

We report in Table 2 the posterior mean of these predicted numbers as our estimator for the expected number of SNPs discovered, together with a 95% credible interval for that number. Although we make an uncommon assumption that none of the effect sizes are exactly zero, our estimates in Table 2 are in the ballpark of the actual numbers from the three cited papers. A clear advantage of using a valid density estimator of true effect sizes in conjunction with the projection formula is that it provides a cheap and simple calculation without carrying out any large-scale experiments. That is, we obtain the density estimator based on the smallest sample size of height study, and quantifies the number of significant SNPs including its uncertainty for larger studies, given no information except their sample sizes. Hence our method can be used to infer the required sample size needed for an expected given number of discoveries.

	Number of individuals		
	133K	253K	700K
Exp. Disc.	134	375	2907
95% C.I.	(125, 143)	(357, 394)	(2790, 3039)

Table 2: Estimated value (Exp.Disc.) and a 95% credible interval (95% C.I.) for predicting the expected number of SNPs discovered as the number of individuals varies. We obtain posterior samples of the predicted number from the projection formula and posterior samples of effect size distribution.

7 Discussion

We have considered the case of nonparametric density deconvolution with possibly heteroscedastic measurement errors, where the true densities are subject to shape constraints, in our case symmetry and unimodality. We are particularly interested in applications where there is a large probability near zero coupled with possibly heavy tailed distributions. We showed that our method, which we call Constrained Bayes Deconvolution, is nonparametrically consistent for estimating the true target density in general, and is particularly well-

equipped for the mixture problem described immediately above. Computationally, it is linear in the sample size, and hence highly scalable.

Mixtures of uniforms are known to contain the Normal variance mixture class (Wang and Pillai, 2013) described in Section 1, and have been utilized in various applications for modeling a symmetric unimodal density. However, the flexibility of such a model depends critically on the flexibility of the mixing distribution. Our carefully designed choice of the Dirichlet process mixture of gammas for this mixing distribution has large support on the space of densities on the positive real line, leads to efficient computation, and is provably consistent. Different approaches, based instead on a number of mixtures of Normals, include Stephens (2016), and a very different approach, based on a computation in Yang et al. (2012), has been taken by Zhang et al. (2018), wherein they fit a regression to a large number of predictors, get the joint regression coefficients, and then do approximations and linear model calculations to reduce to the marginal effects, which in this context is our X . Zhu and Stephens (2017) is a Bayesian approach similar to Zhang et al. (2018). This particular approach (Zhu and Stephens, 2017) seems to be limited to genome-wide association studies based on SNPs, where the linkage disequilibrium (correlation) between the SNPs is known.

While we are not limited to the effect size context, in that context it might be interesting to replace the idea of a large probability near zero to the case of a point mass exactly at zero, which has been done in the mixtures of Normals by Stephens (2016) and Zhang et al. (2018). This is possible to do within our framework and will be reported upon elsewhere. The corresponding results in Table 1 are much the same.

Supplementary Material

The **Supplementary Material** includes a data analysis of a microarray experiment. The R code is available from the last author. Code for simulations are provided at https://github.com/tamustatsy/Constrained_Deconvolution/.

Acknowledgments

Su and Carroll were supported by a grant from the National Cancer Institute (U01-CA057030). Bhattacharya was supported from National Science Foundation grant (NSF DMS 1613156) and a NSF CAREER Award (DMS 1653404). Zhang and Chatterjee were partially funded through a Patient-Centered Outcomes Research Institute (PCORI) Award (ME-1602-34530). The authors were also supported in part by a grant from the National Human Genome Research Institute (R01-HG010480). The statements and opinions in this article are solely the responsibility of the authors and do not necessarily represent the views of PCORI, its Board of Governors or Methodology Committee. The authors are grateful to Aurore Delaigle of the University of Melbourne and her collaborators for publishing R package, `deconvolve`, for homoscedastic and heteroscedastic kernel density deconvolution on Github.

References

- Allen, H. L., Estrada, K., Lettre, G., Berndt, S. I., Weedon, M. N., Rivadeneira, F., Willer, C. J., Jackson, A. U., Vedantam, S., Raychaudhuri, S., et al. (2010). Hundreds of variants clustered in genomic loci and biological pathways affect human height. *Nature*, 467, 832–838.
- Bochkina, N. and Rousseau, J. (2017). Adaptive density estimation based on a mixture of Gammas. *Electronic Journal of Statistics*, 11, 916–962.
- Brunner, L. J. and Lo, A. Y. (1989). Bayes methods for a symmetric unimodal density and its mode. *Annals of Statistics*, 17, 1550–1566.
- Carroll, R. J. and Hall, P. (1988). Optimal rates of convergence for deconvolving a density. *Journal of the American Statistical Association*, 83, 1184–1186.
- Chatterjee, N., Wheeler, B., Sampson, J., Hartge, P., Chanock, S. J., and Park, J.-H. (2013). Projecting the performance of risk prediction based on polygenic analyses of genome-wide association studies. *Nature genetics*, 45, 400.
- Chu, K. C. (1973). Estimation and decision for linear systems with elliptical random processes. *IEEE Transactions on Automatic Control*, 18, 499–505.
- Davidson, L. A., Nguyen, D. V., Hokanson, R. M., Callaway, E. S., Isett, R. B., Turner, N. D., Dougherty, E. R., Wang, N., Lupton, J. R., Carroll, R. J., et al. (2004). Chemopreventive n-3 polyunsaturated fatty acids reprogram genetic signatures during colon cancer initiation and progression in the rat. *Cancer Research*, 64, 6797–6804.
- Delaigle, A. and Meister, A. (2008). Density estimation with heteroscedastic error. *Bernoulli*, 14, 562–579.
- Donnet, S., Rivoirard, V., Rousseau, J., and Scricciolo, C. (2018). Posterior concentration rates for Empirical Bayes procedures, with applications to Dirichlet Process mixtures. *Bernoulli*, 24, 231–256.

- Fan, J. (1991). On the optimal rates of convergence for nonparametric deconvolution problems. *Annals of Statistics*, 19, 1257–1272.
- Feller, W. (1971). *An Introduction to Probability Theory and its Applications*, volume 2. John Wiley & Sons.
- Ferguson, T. S. (1973). A Bayesian analysis of some nonparametric problems. *Annals of Statistics*, 1, 209–230.
- Gao, F. and van der Vaart, A. (2016). Posterior contraction rates for deconvolution of Dirichlet-Laplace mixtures. *Electronic Journal of Statistics*, 10, 608–627.
- Ghosal, S., Ghosh, J. K., and van der Vaart, A. W. (2000). Convergence rates of posterior distributions. *Annals of Statistics*, 28, 500–531.
- Ishwaran, H. and Zarepour, M. (2002). Exact and approximate sum representations for the dirichlet process. *Canadian Journal of Statistics*, 30, 269–283.
- Kalli, M., Griffin, J. E., and Walker, S. G. (2011). Slice sampling mixture models. *Statistics and Computing*, 21, 93–105.
- Nguyen, X. (2013). Convergence of latent mixing measures in finite and infinite mixture models. *Annals of Statistics*, 41, 370–400.
- Purcell, S., Neale, B., Todd-Brown, K., Thomas, L., Ferreira, M. A., Bender, D., Maller, J., Sklar, P., De Bakker, P. I., Daly, M. J., et al. (2007). Plink: a tool set for whole-genome association and population-based linkage analyses. *The American Journal of Human Genetics*, 81, 559–575.
- Sarkar, A., Mallick, B. K., Staudenmayer, J., Pati, D., and Carroll, R. J. (2014). Bayesian semiparametric density deconvolution in the presence of conditionally heteroscedastic measurement errors. *Journal of Computational and Graphical Statistics*, 23, 1101–1125.
- Sarkar, A., Pati, D., Chakraborty, A., Mallick, B. K., and Carroll, R. J. (2017). Bayesian semiparametric multivariate density deconvolution. *Journal of the American Statistical Association*, 112.
- Scricciolo, C. (2018). Bayes and maximum likelihood for L^1 -Wasserstein deconvolution of Laplace mixtures. *Statistical Methods & Applications*, 27, 333–362.
- Sethuraman, J. (1994). A constructive definition of Dirichlet priors. *Statistica Sinica*, 4, 639–650.
- Shen, W., Tokdar, S. T., and Ghosal, S. (2013). Adaptive Bayesian multivariate density estimation with Dirichlet mixtures. *Biometrika*, 100, 623–640.
- Stefanski, L. and Carroll, R. J. (1990). Deconvoluting kernel density estimators. *Statistics*, 21, 165–184.
- Stephens, M. (2016). False discovery rates: a new deal. *Biostatistics*, 18, 275–294.

- Turnbull, B. C. and Ghosh, S. K. (2014). Unimodal density estimation using Bernstein polynomials. *Computational Statistics & Data Analysis*, 72, 13–29.
- Villani, C. (2008). *Optimal Transport: Old and New*, volume 338. Springer Science & Business Media.
- Wang, H. and Pillai, N. S. (2013). On a class of shrinkage priors for covariance matrix estimation. *Journal of Computational and Graphical Statistics*, 22, 689–707.
- West, M. (1987). On scale mixtures of Normal distributions. *Biometrika*, 74, 646–648.
- Wood, A. R., Esko, T., Yang, J., Vedantam, S., Pers, T. H., Gustafsson, S., Chu, A. Y., Estrada, K., Luan, J., Kutalik, Z., et al. (2014). Defining the role of common variation in the genomic and biological architecture of adult human height. *Nature Genetics*, 46, 1173.
- Yang, J., Ferreira, T., Morris, A. P., Medland, S. E., Madden, P. A., Heath, A. C., Martin, N. G., Montgomery, G. W., Weedon, M. N., Loos, R. J., et al. (2012). Conditional and joint multiple-snp analysis of gwas summary statistics identifies additional variants influencing complex traits. *Nature genetics*, 44, 369.
- Yengo, L., Sidorenko, J., Kemper, K. E., Zheng, Z., Wood, A. R., Weedon, M. N., Frayling, T. M., Hirschhorn, J., Yang, J., Visscher, P. M., et al. (2018). Meta-analysis of genome-wide association studies for height and body mass index in 700000 individuals of european ancestry. *Human Molecular Genetics*, 27, 3641–3649.
- Zhang, Y., Qi, G., Park, J.-H., and Chatterjee, N. (2018). Estimation of complex effect-size distributions using summary-level statistics from genome-wide association studies across 32 complex traits. *Nature Genetics*, 50, 1318.
- Zhu, X. and Stephens, M. (2017). Bayesian large-scale multiple regression with summary statistics from genome-wide association studies. *Annals of Applied Statistics*, 11, 1561–1592.

Appendix

A.1 Proof of Theorem 1

Below we provide details to verify (3), (4) and (5) in Section 1.

Bochkina and Rousseau (2017) derive the posterior convergence rate for Dirichlet location-mixture of Gammas in the no-measurement error case. We obtain some preliminary results on the layer of $g(\cdot)$ from their work. It is worth pointing out that since the condition on the Dirichlet process base probability is different from theirs, only results that are not affected by the type of prior can be inherited directly in this article. These results can be obtained by Proposition 2.1 and Lemma B.2 in Bochkina and Rousseau (2017). Any $g_0 \in \mathcal{M}$ can be approximated by convoluting a Gamma kernel and some discrete probability, that is, $K_z * P_N$, where K_z is representing the Gamma kernel with shape and rate parameter $(z, z/\mu)$ and P_N is a discrete probability $P_N = \sum_{j=1}^N p_j \delta_{u_j}$, with $N \leq N_0 \sqrt{z} (\log z)^{3/2}$, $u_j \in [e_z, E_z]$. The sequences $\{u_j\}_{j=1}^N$ and $\{p_j\}_{j=1}^N$ satisfy that $u_1 = e_z$, $u_N = E_z$, $u_{j+1} - u_j > z^{-A}$ and $p_j > z^{-A}$ for some $A > 0$ and with $e_z = z^{-a}$ and $E_z = z^b$, $a > 1$, $b > 1/\rho_1$, the choice of lower bound on b is larger than that used in Bochkina and Rousseau (2017), specifically we require $b > 1/(\rho_1 - 2)$. Define $u_0 = u_1$, $u_{N+1} = u_N$, then $U_j = [(u_j + u_{j-1})/2, (u_j + u_{j+1})/2]$ covers $[e_z, E_z]$. Moreover, $U_0 = \mathbb{R}^+ \setminus \cup_{j=1}^N U_j$.

Under our Dirichlet location-mixture of Gammas model, $g(\theta) = K_z * G(\theta) = \int g_{z, z/\mu}(\theta) dG(\mu)$, where the mixing measure G follows $DP(m, D)$. Define a prior set $\mathcal{G}_z = \{G : G(U_i)/p_i \in (1 - 2z^{-A}, 1 - z^{-A}), i = 1, \dots, N\}$, while $z \in I_n = (z_n, 2z_n)$. The choice of z_n will be specified later.

In Appendix A.1.1 below, we show that on this prior set $\mathcal{G}_z \times I_n$, the following bounds hold,

$$P_0 \log(p_0/p) \lesssim z_n^{-1} \log(z_n), \text{ and } P_0 \{\log(p_0/p)\}^2 \lesssim z_n^{-1} \log(z_n) \log(n). \quad (\text{A.1})$$

In Appendix A.1.2, the lower bound for the prior probability of the prior set $\mathcal{G}_z \times I_n$ is derived, namely that

$$\Pi(\mathcal{G}_z \times I_n) \gtrsim \exp\{C \sum_j \log(\alpha_j)\} \gtrsim \exp\{-C z_n^{B+1/2} (\log z_n)^{3/2}\}, \quad (\text{A.2})$$

where $B = \max(ba_1, aa_0)$.

Take $z_n = n^{2/(2B+3)} (\log n)^{-1/(2B+3)}$, such that $\epsilon_n^2 = z_n^{-1} \log z_n \asymp n^{-2/(2B+3)} (\log n)^{(2B+2)/(2B+3)}$. From (A.1) and (A.2), the prior set $\mathcal{G}_z \times I_n$ has prior probability bounded below by $\exp(-Cn\epsilon_n^2)$ while on this set $P_0 \log(p_0/p) \lesssim \epsilon_n^2$, $P_0 \{\log(p_0/p)\}^2 \lesssim \epsilon_n^2 \log n$. Therefore, the prior concentration inequality (5) holds.

Under the prior in Condition 3 and the ϵ_n just defined, the sieve space on $p(\cdot)$, \mathcal{F}_n , in (3) and (4) will be defined as follows. Consider a subspace of \mathcal{G} ,

$$Q = Q(\epsilon, J, a, b, \underline{z}, \bar{z}) = \{g(\cdot) = \sum_{j=1}^{\infty} \pi_j g_{z, z/\mu_j}(\cdot) : \sum_{j>J} \pi_j < \epsilon, z \in [\underline{z}, \bar{z}], \mu_j \in [a, a+b] \\ \text{for } j = 1, \dots, J\}.$$

The sieve space of \mathcal{G} is given by $Q_n = Q(\zeta\epsilon_n, J_n, a_n, b_n, \underline{z}_n, \bar{z}_n)$. Because of the multi-layer relationship between $p(\cdot)$, $f(\cdot)$ and $g(\cdot)$ from the definition of $p(\cdot)$ and $f(\cdot)$, the sieve space on $p(\cdot)$, \mathcal{F}_n , is defined naturally based on Q_n . Furthermore, the entropy and prior mass conditions, (3) and (4), for Q_n can be passed along to \mathcal{F}_n due to the fact that the Hellinger distance between any two functions $g_1, g_2 \in \mathcal{G}$ is greater than or equal to that between the corresponding p_1, p_2 , that is, $h^2(p_1, p_2) \leq h^2(g_1, g_2)$. It remains to show that Q_n satisfies (3) and (4).

According to Lemma 4.2 in Bochkina and Rousseau (2017), (4) holds for Q_n if for some positive constant c ,

$$J_n D\{(0, a_n)\} \lesssim \exp(-c n \epsilon_n^2), \quad J_n D\{(a_n + b_n, \infty)\} \lesssim \exp(-c n \epsilon_n^2), \\ 1 - \Pi_z([\underline{z}_n, \bar{z}_n]) \lesssim \exp(-c n \epsilon_n^2), \quad \{em J_n^{-1} \log(1/\epsilon_n)\}^{J_n} \lesssim \exp(-c n \epsilon_n^2). \quad (\text{A.3})$$

Equation (3) holds for Q_n if

$$J_n \{\log \log(b_n/a_n) + \log(\bar{z}_n) + \log(1/\epsilon_n)\} + \log \log(\bar{z}_n/\underline{z}_n) \lesssim n \epsilon_n^2. \quad (\text{A.4})$$

For notational simplicity, let $\eta = 2B + 3$, and set $C > 0$ as a large enough constant. These conditions are met (details can be found in Appendix A.1.3) for the following choices of $J_n = C n^{(2B+1)/\eta} (\log n)^{-1/\eta}$, $a_n = C \{n^{(2B+1)/\eta} (\log n)^{(2B+2)/\eta}\}^{-1/a'_0}$, $b_n = C \{n^{(2B+1)/\eta} (\log n)^{(2B+2)/\eta}\}^{1/a'_1}$, $\underline{z}_n = 1 + \exp\{-C n^{(2B+1)/\eta} (\log n)^{(2B+2)/\eta}\}$, $\bar{z}_n = C n^{2(2\beta+1)/\eta} (\log n)^{2\{(2B+2)/\eta - \rho_z\}}$.

A.1.1 Kullback-Leibler Bound

One useful result from Bochkina and Rousseau (2017) (in the proof of their Lemma B.3) is that for any z , and $G \in \mathcal{G}_z = \{G : G(U_i)/p_i \in (1 - 2z^{-A}, 1 - z^{-A}), i = 1, \dots, N\}$, it is proved that $h^2(g_0, g) \lesssim z^{-1}$, where $g = K_z * G$. Moreover, it has been shown (in the proof of their

Lemma B.3) that $g(\theta) = (K_z * G)(\theta)$ satisfies

$$g(\theta) \gtrsim \begin{cases} z^{-A+1/2-M^2/2} & \theta \in [e_z, E_z], \\ \exp\{2z \log(\theta/e_z) - c \log z\} & \theta < e_z, \\ \exp(-2z\theta/e_z) & \theta > E_z. \end{cases} \quad (\text{A.5})$$

Bochkina and Rousseau (2017) also contains the following lemma (Lemma C.2 in their paper) which we will make use of to find the tail probability of the integral with respect to g , which is stated as Lemma A.2 below.

Lemma A.1. *For all $\delta \in (0, 1)$ there exists $c(\delta) > 0$ such that for all z large enough and $u < 1 - \delta$,*

$$\frac{z^z \exp(-z/u)}{\Gamma(z)u^z} \leq \exp\{-c(\delta)z/u\}.$$

Now we state our Lemma which makes use of Lemma A.1 to bound the tail probability of the integral with respect to g . The proof is given in Section A.3.

Lemma A.2. *For all z large enough such that Lemma A.1 holds, we have*

$$\int_{\theta < 2E_z} g(\theta) d\theta \geq 1 - z^{-1} \exp\{-2c(0.5)z\} - z^{-A}.$$

The following inequality, by Lemma 4 of Shen et al. (2013), can be used to bound the quantities $P_0 \log(p_0/p)$ and $P_0 \{\log(p_0/p)\}^2$. There exists a λ_0 such that for any $\lambda \in (0, \lambda_0)$ and any two densities p and q (P denotes the probability distribution with respect to p),

$$P \log(p/q) \leq h^2(p, q)(1 - 2 \log \lambda) + 2P\{\log(p/q)I(q/p \leq \lambda)\}, \quad (\text{A.6})$$

$$P\{\log(p/q)\}^2 \leq h^2(p, q)\{12 + 2(\log \lambda)^2\} + 8P[\{\log(p/q)\}^2 I(q/p \leq \lambda)]. \quad (\text{A.7})$$

We will use ϕ_σ to denote a Normal density with mean zero and standard deviation σ . Since

$$\begin{aligned} \int f^{1/2}(u) f_0^{1/2}(u) du &= \int \int \phi_\sigma(w - u) f^{1/2}(u) f_0^{1/2}(u) du dw \\ &\leq \int \left\{ \int \phi_\sigma(w - u) f(u) du \right\}^{1/2} \left\{ \int \phi_\sigma(w - u) f_0(u) du \right\}^{1/2} dw \\ &= \int p^{1/2}(w) p_0^{1/2}(w) dw. \end{aligned} \quad (\text{A.8})$$

$$\begin{aligned} \int g^{1/2}(\theta) g_0^{1/2}(\theta) d\theta &\leq \int \int (2\theta)^{-1} I_{(-\theta \leq u < \theta)} g^{1/2}(\theta) g_0^{1/2}(\theta) d\theta du \\ &\leq \int \left\{ \int (2\theta)^{-1} I_{(-\theta \leq u \leq \theta)} g(\theta) d\theta \right\}^{1/2} \int \left\{ (2\theta)^{-1} I_{(-\theta \leq u \leq \theta)} g_0(\theta) d\theta \right\}^{1/2} du \\ &= \int f^{1/2}(u) f_0^{1/2}(u) du. \end{aligned} \quad (\text{A.9})$$

Making use of (A.8) and (A.9), together with the fact that $1-h^2(p_1, p_2)/2 = \int p_1^{1/2}(x)p_2^{1/2}(x)dx$ holds for any two integrable functions p_1, p_2 and the previous result from Bochkina and Rousseau (2017) about $h^2(g, g_0)$, we obtain that

$$h^2(p, p_0) \lesssim z^{-1}. \quad (\text{A.10})$$

Suppose $p_0(\cdot)$ has an upper bound K . For $|w| < E_z - \delta_N - z^{-A}$, where $\delta_N = u_N - u_{N-1} > z^{-A}$,

$$\begin{aligned} p(w)/p_0(w) &\geq K\sigma^{-1} \int_{w-z^{-A}}^{w+z^{-A}} \exp(-(w-u)^2/\sigma^2) \int_{|u|}^{\infty} \theta^{-1}g(\theta)d\theta du \\ &\geq 2K\sigma^{-1}z^{-A} \exp(-z^{-2A}/\sigma^2) \int_{|w|+z^{-A}}^{\infty} \theta^{-1}g(\theta)d\theta \\ &\geq 2K\sigma^{-1}z^{-A} \exp(-z^{-2A}/\sigma^2) \int_{E_z-\delta_N}^{\infty} \theta^{-1}g(\theta)d\theta \\ &\gtrsim z^{-A} \int_{E_z-\delta_N}^{E_z} \theta^{-1}g(\theta)d\theta \\ &\gtrsim E_z^{-1}z^{-A+1/2-M^2/2}z^{-A}z^{-A} = z^{-3A-b+1/2-M^2/2}. \end{aligned} \quad (\text{A.11})$$

The last inequality is a result of (A.5).

On the other hand, when $|w| > E_z - \delta_N - z^{-A}$, so that when z is large, $w^2 > E_z^2/2$,

$$\begin{aligned} p(w)/p_0(w) &\geq K\sigma^{-1} \int_{|u|\leq 2E_z} \exp(-(w-u)^2/\sigma^2) \int_{|u|}^{\infty} \theta^{-1}g(\theta)d\theta du \\ &\geq K\sigma^{-1} \exp(-18w^2/\sigma^2) \int_{\theta\leq 2E_z} g(\theta)d\theta \\ &\geq K\sigma^{-1}[1 - z^{-1} \exp\{-2c(0.5)z\} - z^{-A}] \exp(-18w^2/\sigma^2). \end{aligned} \quad (\text{A.12})$$

According to (A.11), for $\lambda = K'z^{-3A-b+1/2-M^2/2}$, if K' is small enough, $\{w : p(w)/p_0(w) \leq \lambda\} \subset \{|w| > E_z - \delta_N - z^{-A}\}$. On the latter set, p_0/p is upper bounded as shown in (A.12). Therefore,

$$P_0[\{\log(p_0/p)\}^2 I(p/p_0 \leq \lambda)] \lesssim \int_{|w|>E_z-\delta_N-z^{-A}} w^4 p_0(w) dw. \quad (\text{A.13})$$

Our next result, Lemma A.3, is proved in Section A.3.

Lemma A.3. Under Condition 2, when t is large, $\int_t^\infty w^4 p_0(w) dw \lesssim t^{-\rho_1+2}$.

Immediately, Lemma A.3 leads to an upper bound of (A.13),

$$P_0[\{\log(p_0/p)\}^2 I(p/p_0 \leq \lambda)] \lesssim z^{-b(\rho_1-2)} \leq z^{-1}, \quad (\text{A.14})$$

the last inequality making use of the property of b that $b > 1/(\rho_1 - 2)$.

Based on (A.10) and (A.14), we can apply (A.6) and (A.7) with the choices of λ the same as the one used in (A.13), $p = p_0$ and $q = p$, and derive that

$$P_0 \log(p_0/p) \lesssim z^{-1} \log(z); \quad P_0 \{\log(p_0/p)\}^2 \lesssim z^{-1} \log(z) \log(n). \quad (\text{A.15})$$

In summary, (A.15) holds whenever $g \in \mathcal{G}_z$, for any z . Hence on the prior set $\mathcal{G}_z \times I_n$, $P_0 \log(p_0/p) \lesssim z_n^{-1} \log(z_n)$, $P_0 \{\log(p_0/p)\}^2 \lesssim z_n^{-1} \log(z_n) \log(n)$.

A.1.2 Prior Probability Bound

Under the new set of priors in Condition 3, the prior probability of the prior set $\mathcal{G}_z \times I_n$ has to be modified in the following way. The techniques in Bochkina and Rousseau (2017) still apply. The only modification lies in the rate of $\alpha_j = mD(U_j)$, $j = 0, \dots, N$. Note that for large $u_{j-1} \gtrsim E_z$,

$$\alpha_j = m \int_{(u_{j-1}+u_j)/2}^{(u_j+u_{j+1})/2} d(u) du \gtrsim C \int_{(u_{j-1}+u_j)/2}^{(u_j+u_{j+1})/2} \exp(-u^{a_1}) du \gtrsim C \exp(-E_z^{a_1}) = C \exp(-z^{ba_1}).$$

For small $0 < u_{j+1} \lesssim e_z$,

$$\alpha_j = m \int_{(u_{j-1}+u_j)/2}^{(u_j+u_{j+1})/2} d(u) du \gtrsim C \int_{(u_{j-1}+u_j)/2}^{(u_j+u_{j+1})/2} \exp(-u^{-a_0}) du \gtrsim C \exp(-e_z^{-a_0}) = C \exp(-z^{aa_0}).$$

Denote $B = \max(ba_1, aa_0)$. For simplicity, we assume without loss of generality that $B = ba_1$. From the above results, $\sum_j (-\log \alpha_j) \lesssim Nz^B \asymp z^{B+1/2} (\log z)^{3/2}$. Then we can repeat the lines in the proof of Lemma 4.1 in Bochkina and Rousseau (2017), so that for $z \in I_n$,

$$\Pi(\mathcal{G}_z) \gtrsim \exp\left\{C \sum_j \log(\alpha_j)\right\} \gtrsim \exp\left\{-Cz_n^{B+1/2} (\log z_n)^{3/2}\right\}.$$

On the other hand,

$$\Pi_z(I_n) \gtrsim \exp\left\{-C\sqrt{z_n} (\log z_n)^{\rho_z}\right\}.$$

A.1.3 Verification of (3) and (4) on the Sieve Space Q_n

In this section, we are going to verify the set of inequalities (A.3) and (A.4) in Appendix A.1. Again, our choices of the sieve space parameters are $J_n = Cn^{(2B+1)/\eta} (\log n)^{-1/\eta}$, $a_n = C\{n^{(2B+1)/\eta} (\log n)^{(2B+2)/\eta}\}^{-1/a'_0}$, $b_n = C\{n^{(2B+1)/\eta} (\log n)^{(2B+2)/\eta}\}^{1/a'_1}$, $\underline{z}_n = 1 + \exp\{-Cn^{(2B+1)/\eta} (\log n)^{(2B+2)/\eta}\}$, and $\bar{z}_n = Cn^{2(2\beta+1)/\eta} (\log n)^{2(2B+2)/\eta - \rho_z}$.

Plugging these values together with the condition on the prior,

$$\begin{aligned}
J_n D\{(0, a_n)\} &= C n^{(2B+1)/\eta} (\log n)^{-1/\eta} \int_0^{a_n} d(u) du \\
&\lesssim n^{(2B+1)/\eta} (\log n)^{-1/\eta} \exp(-a_n^{-a'_0}) \lesssim \exp(-c n \epsilon_n^2); \\
J_n D\{(a_n + b_n, \infty)\} &= C n^{(2B+1)/\eta} (\log n)^{-1/\eta} \int_{a_n+b_n}^{\infty} d(u) du \\
&\lesssim n^{(2B+1)/\eta} (\log n)^{-1/\eta} \exp(-b_n^{a'_1}) \lesssim \exp(-c n \epsilon_n^2); \\
\Pi_z\{(1, \underline{z}_n)\} &\lesssim (\underline{z}_n - 1)^{c_0} \lesssim \exp(-c n \epsilon_n^2); \\
\Pi_z\{\{\bar{z}_n, \infty\}\} &\lesssim \exp(-c' \sqrt{\bar{z}_n} (\log \bar{z}_n)^{\rho_z}) \lesssim \exp(-c n \epsilon_n^2).
\end{aligned}$$

To see that $\{em J_n^{-1} \log(1/\epsilon_n)\}^{J_n} \lesssim \exp(-c n \epsilon_n^2)$, it is sufficient to show that

$$J_n [\log(J_n) - \log \log(n) + C] \gtrsim c n^{(2B+1)/\eta} (\log n)^{(2B+2)/\eta},$$

which holds for $J_n = C n^{(2B+1)/\eta} (\log n)^{-1/\eta}$.

Lastly, we can easily check that the sufficient inequality for (3) is valid,

$$J_n [\log \log(b_n/a_n) + \log(\bar{z}_n) + \log(1/\epsilon_n)] + \log \log(\bar{z}_n/\underline{z}_n) \lesssim n \epsilon_n^2.$$

A.2 Proof of Lemma 1

Denote K as a symmetric density, whose Fourier transform \widehat{K} has support $[-1, 1]$. Moreover, K has bounded moments up to order s ($s > 2$). Let $K_\delta(\cdot) = \delta^{-1} K(\cdot/\delta)$ be its mollifier. Let g_δ be a function whose Fourier transform \widehat{g}_δ equals $\widehat{K}_\delta/\widehat{\phi}_\sigma$, the ratio between the Fourier transform of the kernel K_δ and that of the Gaussian kernel ϕ_σ .

By the triangular inequality,

$$W_2^2(f, f_0) \lesssim W_2^2(f, f * K_\delta) + W_2^2(f_0, f_0 * K_\delta) + W_2^2(f * K_\delta, f_0 * K_\delta). \quad (\text{A.16})$$

For the first and second term, based on the property of Wasserstein distance and convolution, the techniques in Nguyen (2013) can be used to show that $W_2^2(f, f * K_\delta) \lesssim \delta^2$, $W_2^2(f_0, f_0 * K_\delta) \lesssim \delta^2$.

For the third term in (A.16), we first follow the route in Lemma 7 of Gao and van der Vaart (2016) which makes use of Theorem 6.15 in Villani (2008) stating that the Wasserstein distance $W_k(H_1, H_2)$ is upper bounded by a multiple of the k th root of $\int |x|^k d|H_1 - H_2|(x)$,

$$W_2^2(f * K_\delta, f_0 * K_\delta) \lesssim \left(\int_{|x| \leq M} + \int_{|x| > M} \right) |x|^2 |(f - f_0) * K_\delta(x)| dx = T_1 + T_2,$$

say. We will work on T_1 and T_2 separately.

By the Cauchy Schwartz inequality,

$$T_1 \leq M^{2+1/2} \|f * K_\delta - f_0 * K_\delta\|_2.$$

Using the arguments in Corollary 2 of Donnet et al. (2018),

$$\begin{aligned} \|f * K_\delta - f_0 * K_\delta\|_2 &= \|(f * \phi_\sigma) * g_\delta - (f_0 * \phi_\sigma) * g_\delta\|_2 = \|p * g_\delta - p_0 * g_\delta\|_2 \\ &\leq \|p - p_0\|_1 \|g_\delta\|_2 \lesssim \|p - p_0\|_1 \exp(\sigma^2 \delta^{-2}/2). \end{aligned}$$

On the other hand,

$$\begin{aligned} T_2 &\leq M^{-(s-2)} \int_{|x|>M} |x|^s [(f + f_0) * K_\delta(x)] dx \\ &\lesssim M^{-(s-2)} \int \int (|x-y|^s + |y|^s) (f + f_0)(x-y) K_\delta(y) dx dy \\ &\lesssim M^{-(s-2)} \int |y|^s K_\delta(y) dy + M^{-(s-2)} \int |x|^s (f + f_0)(x) dx. \end{aligned}$$

The s th moment of K_δ is finite according to the assumption on K , moreover, the s th moment of f_0 is also finite under the fact that the s th moment of f_0 is equivalent to the s th moment of g_0 and Condition 2 whenever $s \leq 4$. To make precise what the upper bound for T_2 is, it remains to check the s th moment of f .

We consider $f(x) = \int I_{(|x|<\theta)}(2\theta)^{-1} g(\theta) d\theta$, with g in the sieve space Q_n in Section 3.2.

$$\begin{aligned} \int |x|^s f(x) dx &= \int |x|^s \int I_{(|x|<\theta)}(2\theta)^{-1} g(\theta) d\theta dx = \int \left(\int |x|^s I_{(|x|<\theta)} dx \right) (2\theta)^{-1} g(\theta) d\theta \\ &\asymp \int \theta^s g(\theta) d\theta = \sum_j \pi_j (z/\mu_j)^{-s} \Gamma(z+s)/\Gamma(z) \lesssim b_n^s, \end{aligned}$$

the last \lesssim is because μ_j has the upper bound $b_n = C \{n^{(2B+1)/\eta} (\log n)^{(2B+2)/\eta}\}^{(1/a'_1)}$.

Plugging the pieces into (A.16),

$$W_2^2(f, f_0) \lesssim \delta^2 + M^{2+1/2} \exp(\sigma^2 \delta^{-2}/2) \|p - p_0\|_1 + M^{-(s-2)} b_n^s. \quad (\text{A.17})$$

The next Lemma is used to select the choice of M in (A.17).

Lemma A.4. *As long as ρ_1 and a'_1 are large enough, there exist some $\nu_1, \nu_2 > 0$ $M = \|p - p_0\|_1^{-2/5+\nu_1}$ such that $M^{-(s-2)} b_n^s = o_p(\|p - p_0\|_1^{\nu_2})$.*

From Lemma A.4, we can take $M = \|p - p_0\|_1^{-2/5+\nu_1}$. In (A.17) the optimal value is achieved at $\delta \asymp \{-\log(M^{5/2} \|p - p_0\|_1)\}^{-1/2} \asymp \{-\log(\|p - p_0\|_1)\}^{-1/2}$. With this choice of M and δ , the second and third term are of order $o(\|p - p_0\|_1^{\nu_1})$ and $o_p(\|p - p_0\|_1^{\nu_2})$, both are of smaller order than the first term $\delta^2 \asymp \{-\log(\|p - p_0\|_1)\}^{-1}$. Thus we have established that $W_2^2(f, f_0) \lesssim \{-\log(\|p - p_0\|_1)\}^{-1}$ whenever g is in the sieve space Q_n .

Remark A.3. From Condition 2, the tail of g_0 needs to decrease with a higher order as ρ_1 increases.

Proof of Lemma A.4. We have shown in Theorem 1 that $\|p - p_0\|_1 = O_p(\epsilon_n)$, where $\epsilon_n = n^{-1/\eta}(\log n)^{(2B+2)/(2\eta)}$, and $\eta = 2B + 3$. It is sufficient to prove $b_n^{s/(s-2)} = o(\epsilon_n^{-2/5+\nu})$ for some $\nu > 0$. From the value of b_n and ϵ_n , $b_n^{s/(s-2)} = o(\epsilon_n^{-2/5+\nu})$ holds if $(2B + 1)s/\{a'_1(s - 2)\} < (2/5 - \nu)$ for some $\nu > 0$. The latter is equivalent to $(2B + 1)s/\{a'_1(s - 2)\} < 2/5$. Since $B = ba_1$, $b > 1/\rho_1$, after some manipulation it becomes

$$a'_1 > \{s/(s - 2)\}(5/2 + 5a_1/\rho_1)$$

Recall the natural relation $a_1 > a'_1$. A large value for ρ_1 and a'_1 will guarantee the validity of the above inequality. \square

A.3 Proofs of Lemmas A.2 and A.3

Proof of Lemma A.2. Recall that $g_{z,\mu}$ denotes a Gamma density with shape z and rate z/μ .

$$\begin{aligned} \int_{\theta < 2E_z} g(\theta) d\theta &= 1 - \int_{\theta > 2E_z} g(\theta) d\theta \\ &= 1 - \int_{\theta > 2E_z} \int_{\mu < E_z} g_{z,\mu}(\theta) dG(\mu) d\theta - \int_{\theta > 2E_z} \int_{\mu > E_z} g_{z,\mu}(\theta) dG(\mu) d\theta \\ &= 1 - \mathbf{I} - \mathbf{II}, \text{ namely.} \end{aligned} \tag{A.18}$$

Apply Lemma A.1 to $g_{z,\mu}(\theta)$ with $\theta > 2E_z$, $\mu < E_z$ such that $\delta = 1/2$,

$$\begin{aligned} \mathbf{I} &\leq \int_{\theta > 2E_z} \theta^{-1} \exp\{-c(0.5)z\theta/E_z\} d\theta \\ &\lesssim E_z^{-1} \int_{\theta > 2E_z} \exp\{-c(0.5)z\theta/E_z\} d\theta = z^{-1} \exp\{-2c(0.5)z\}. \end{aligned} \tag{A.19}$$

On the other hand, for any $G \in \mathcal{G}_z$, $G(\mu > E_z) \leq z^{-A}$, hence

$$\mathbf{II} \leq \int_{\theta > 2E_z} g_{z,E_z}(\theta) d\theta \int_{\mu > E_z} dG(\mu) \lesssim z^{-A}. \tag{A.20}$$

Combining (A.18), (A.19) and (A.20), the desired result is proved. \square

Proof of Lemma A.3. Throughout the proof, we assume that t is any large number.

Since $W^4 \leq C(X^4 + U^4)$, $P_0(W > t) \leq P_0(X > t/2) + P_0(U > t/2)$,

$$P_0\{W^4 I_{(|W|>t)}\} \lesssim P_0\{X^4 I_{(|X|>t/2)}\} + P_0\{U^4 I_{(|U|>t/2)}\} + P_0\{X^4 I_{(|U|>t/2)}\} + P_0\{U^4 I_{(|X|>t/2)}\}. \tag{A.21}$$

Under Condition A.3, it can be easily shown that $P_0(X^4) < \infty$. Moreover, the fourth moment of Normal distribution exists, therefore, $P_0(U^4) < \infty$. It follows that the second and third term in (A.21) are upper bounded by the first and fourth term correspondingly, thus

$$P_0\{W^4 I_{(|W|>t)}\} \lesssim P_0\{X^4 I_{(|X|>t/2)}\} + P_0\{U^4 I_{(|U|>t/2)}\}. \quad (\text{A.22})$$

Since U follows a Normal distribution which has exponential tail, $P_0\{U^4 I_{(|U|>t/2)}\} \lesssim t^{-\rho_1+2}$. For the proof of the Lemma, it remains to show the upper bound of the first term on the right hand side of (A.22).

$$\begin{aligned} P_0\{X^4 I_{(|X|>t/2)}\} &= P_0[P_0\{X^4 I_{(|X|>t/2)}|\theta\}] = \int (2\theta)^{-1} \int x^4 I_{\{|x|>t/2\} \cap \{|x|<\theta\}} dx g_0(\theta) d\theta \\ &\lesssim \int \theta^{-1} I_{(|\theta|>t/2)} \{\theta^5 - (t/2)^5\} g_0(\theta) d\theta \\ &\leq \int \theta^4 I_{(|\theta|>t/2)} g_0(\theta) d\theta \lesssim (1+t/2)^{-\rho_1+2} \lesssim t^{-\rho_1+2}. \end{aligned}$$

The second but last inequality is because of Condition 2. This concludes the proof of Lemma A.3. \square

A.4 Major differences in proofs when the error is Laplace

We walk through the steps in Section A.1 and A.2 to prove Theorem 1 and Lemma 2 correspondingly. Theorem 2 is again a corollary of the two. Let us denote $\psi_\sigma = (2\sigma)^{-1} \exp(-|x|/\sigma)$ as the density of Laplace distribution with location zero and scale parameter σ .

Theorem 1 can be shown by modifying Section A.1. We can directly show that only when deriving the KL type upper bounds in (A.1) the error distribution might play a role. However, it turns out (A.1) is not changing based on the details below.

The lines in (A.8) and (A.9) go through for any density, in particular ψ_σ . So from (A.10) it remains true that $h^2(p, p_0) \lesssim z^{-1}$.

Also, the lower bound (A.11) for $p(w)/p_0(w)$ on $|w| < E_z - \delta_N - z^{-A}$ stays the same, while the lower bound (A.12) for $p(w)/p_0(w)$ on $|w| > E_z - \delta_N - z^{-A}$ changes slightly to $K\sigma^{-1}[1 - z^{-1} \exp\{-2c(0.5)z\} - z^{-A}] \exp(-4|w|/\sigma)$. These bounds would yield the upper bounds for the KL-type divergence, for $\lambda = K' z^{-3A-b+1/2-M^2/2}$ (K' small enough),

$$\begin{aligned} P_0\{\log(p_0/p) I(p/p_0 \leq \lambda)\} &\lesssim \int_{|w|>E_z-\delta_N-z^{-A}} |w| p_0(w) dw, \\ P_0\{[\log(p_0/p)]^2 I(p/p_0 \leq \lambda)\} &\lesssim \int_{|w|>E_z-\delta_N-z^{-A}} w^2 p_0(w) dw. \end{aligned}$$

Under condition 2' we can show that, along the same lines of proofs for Lemma A.3, both terms on the right hand side above are bounded by z^{-1} . Hence $P_0\{\log(p_0/p)I(p/p_0 \leq \lambda)\} \lesssim z^{-1}$, $P_0[\{\log(p_0/p)\}^2 I(p/p_0 \leq \lambda)] \lesssim z^{-1}$. Thus (A.1) concludes.

Lemma 2 can be shown by modifying Section A.2. We revise the definition of g_δ whose Fourier transform \widehat{g}_δ equals $\widehat{K}_\delta/\widehat{\psi}_\sigma$, the ratio between the Fourier transform of the kernel K_δ and that of the Laplace density ψ_σ .

As shown in Section A.2, the upper bound (up to constant) for the term $\|f*K_\delta - f_0*K_\delta\|_2$ is $\|p - p_0\|_1 \|g_\delta\|_2$. The L_2 norm of $\|g_\delta\|_2$ is the same as the L_2 norm its Fourier transform, which is bounded by $(1 + \sigma^2\delta^{-2})\delta^{-1/2} \asymp \delta^{-5/2}$.

So (A.17) (the other two terms are not affected by distribution of error) is modified to

$$W_2^2(f, f_0) \lesssim \delta^2 + M^{2+1/2}\delta^{-5/2}\|p - p_0\|_1 + M^{-(s-2)}b_n^s.$$

Lemma A.4 still holds for the same choice of M , that is, there exists $\nu_1, \nu_2 > 0$ such that $M = \|p - p_0\|_1^{-2/5+\nu_1}$ and $M^{-(s-2)}b_n^s = o_p(\|p - p_0\|_1^{\nu_2})$ given that ρ_1 and a'_1 are large enough. Then we can show that the right hand side of the above is $O(\|p - p_0\|_1^\nu)$. However, the value of ν is determined by the interplay of ρ_1 and a'_1 and does not have a simple form so we omit writing it out.

		Normal		Laplace	
n		Constrained	Kernel	Constrained	Kernel
		Bayes		Bayes	
1000	IAE	0.107 (0.016)	0.349 (0.105)	0.104 (0.012)	0.185 (0.046)
	ISE	0.072 (0.019)	0.148 (0.043)	0.067 (0.012)	0.079 (0.022)
	W_2	0.165 (0.050)	0.589 (0.209)	0.185 (0.054)	0.285 (0.068)
5000	IAE	0.091 (0.014)	0.277 (0.047)	0.081 (0.013)	0.127 (0.028)
	ISE	0.072 (0.014)	0.120 (0.022)	0.062 (0.013)	0.055 (0.015)
	W_2	0.073 (0.017)	0.445 (0.122)	0.076 (0.019)	0.185 (0.038)

Table 3: Comparison of our Constrained Bayes Deconvolution method (Constrained Bayes) and the deconvoluting kernel density estimator (Kernel). This is in the case when the target density is a t-density with 5 degrees of freedom and the measurement errors are from Normal or Laplace distribution with homoscedastic variance. The sample size is n , IAE is integrated absolute error, and ISE is integrated squared error. W_2 denotes the Wasserstein distance of order 2. Numbers in parentheses are standard errors. Sample sizes greater than 5000 yield similar results.

		Normal		Laplace	
		Constrained Bayes	Kernel	Constrained Bayes	Kernel
1000	IAE	0.086 (0.010)	0.394 (0.045)	0.089 (0.010)	0.220 (0.046)
	ISE	0.053 (0.007)	0.183 (0.023)	0.052 (0.006)	0.098 (0.024)
	W_2	0.140 (0.042)	0.456 (0.060)	0.154 (0.039)	0.324 (0.070)
5000	IAE	0.057 (0.007)	0.389 (0.022)	0.062 (0.007)	0.189 (0.056)
	ISE	0.035 (0.005)	0.181 (0.012)	0.038 (0.004)	0.085 (0.027)
	W_2	0.076 (0.014)	0.430 (0.032)	0.083 (0.016)	0.279 (0.052)

Table 4: Comparison of our Constrained Bayes Deconvolution method (Constrained Bayes) and the deconvoluting kernel density estimator (Kernel). This is in the case when the target density is a t-density with 5 degrees of freedom and the measurement errors are from Normal or Laplace distribution with heteroscedastic variance. The sample size is n , IAE is integrated absolute error, and ISE is integrated squared error. W_2 denotes the Wasserstein distance of order 2. Numbers in parentheses are standard errors. Sample sizes greater than 5000 yield similar results.

		Normal		Laplace	
		Constrained Bayes	Kernel	Constrained Bayes	Kernel
1000	IAE	0.326 (0.054)	0.720 (0.115)	0.258 (0.044)	0.393 (0.078)
	ISE	0.390 (0.065)	0.572 (0.083)	0.307 (0.054)	0.309 (0.075)
	W_2	0.109 (0.026)	0.263 (0.075)	0.086 (0.020)	0.136 (0.029)
	Exceedance	0.068 (0.021)	0.178 (0.048)	0.049 (0.016)	0.047 (0.025)
5000	IAE	0.188 (0.033)	0.656 (0.059)	0.139 (0.018)	0.280 (0.049)
	ISE	0.219 (0.038)	0.530 (0.046)	0.167 (0.019)	0.217 (0.049)
	W_2	0.057 (0.011)	0.222 (0.032)	0.041 (0.011)	0.087 (0.018)
	Exceedance	0.026 (0.010)	0.146 (0.019)	0.014 (0.008)	0.023 (0.014)

Table 5: Comparison of our Constrained Bayes Deconvolution method (Constrained Bayes), the deconvoluting kernel density estimator (Kernel). This is in the case when the target density is a mixture of t-density with 5 degrees of freedom and a Normal density with standard deviation 0.2, and when the measurement errors are from Normal or Laplace distribution with homoscedastic variance. The sample size is n , IAE is integrated absolute error, ISE is integrated squared error and Exceedance is the absolute difference between the exceedance probability under the estimated and true densities. W_2 denotes the Wasserstein distance of order 2. Numbers in parentheses are standard errors. Sample sizes greater than 5000 yield similar results.

		Normal		Laplace	
n		Constrained Bayes	Kernel	Constrained Bayes	Kernel
1000	IAE	0.452 (0.067)	0.848 (0.053)	0.359 (0.058)	0.473 (0.067)
	ISE	0.532 (0.073)	0.656 (0.033)	0.422 (0.066)	0.374 (0.084)
	W_2	0.176 (0.036)	0.360 (0.085)	0.147 (0.030)	0.183 (0.051)
	Exceedance	0.121 (0.027)	0.259 (0.040)	0.092 (0.021)	0.071 (0.048)
5000	IAE	0.276 (0.047)	0.820 (0.024)	0.183 (0.028)	0.357 (0.091)
	ISE	0.321 (0.057)	0.639 (0.014)	0.211 (0.029)	0.279 (0.080)
	W_2	0.100 (0.017)	0.309 (0.053)	0.083 (0.017)	0.140 (0.058)
	Exceedance	0.065 (0.013)	0.231 (0.018)	0.048 (0.010)	0.049 (0.047)

Table 6: Comparison of our Constrained Bayes Deconvolution method (Constrained Bayes), the deconvoluting kernel density estimator (Kernel). This is in the case when the target density is a mixture of t-density with 5 degrees of freedom and a Normal density with standard deviation 0.2, and when the measurement errors are from Normal or Laplace distribution with heteroscedastic variance. The sample size is n , IAE is integrated absolute error, ISE is integrated squared error and Exceedance is the absolute difference between the exceedance probability under the estimated and true densities. W_2 denotes the Wasserstein distance of order 2. Numbers in parentheses are standard errors. Sample sizes greater than 5000 yield similar results.

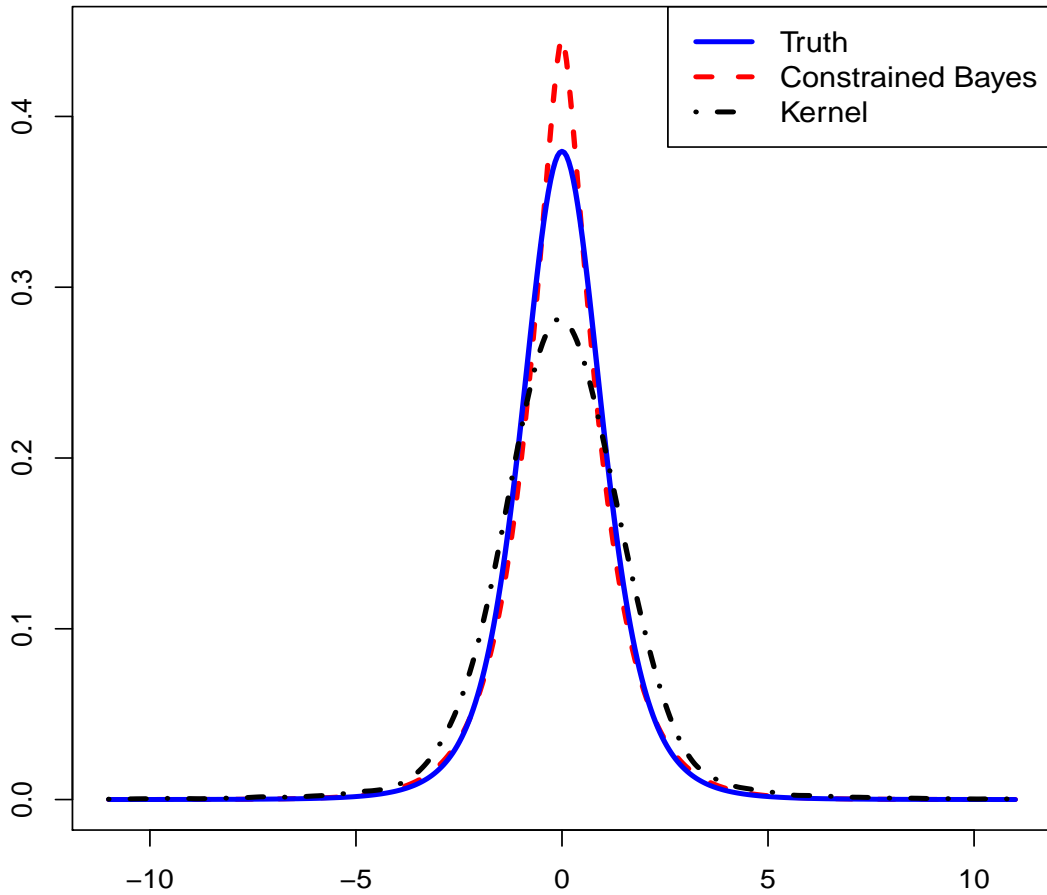


Figure 1: Mean density estimates for the homoscedastic Normal measurement error simulation of Section 5.2 for sample size $n = 5000$. Solid blue line is the truth (Truth, a t -density with 5 degrees of freedom), the dashed red line is our Constrained Bayes Deconvolution method (Constrained Bayes) and the dash-dotted black line is the deconvoluting kernel density estimator (Kernel).

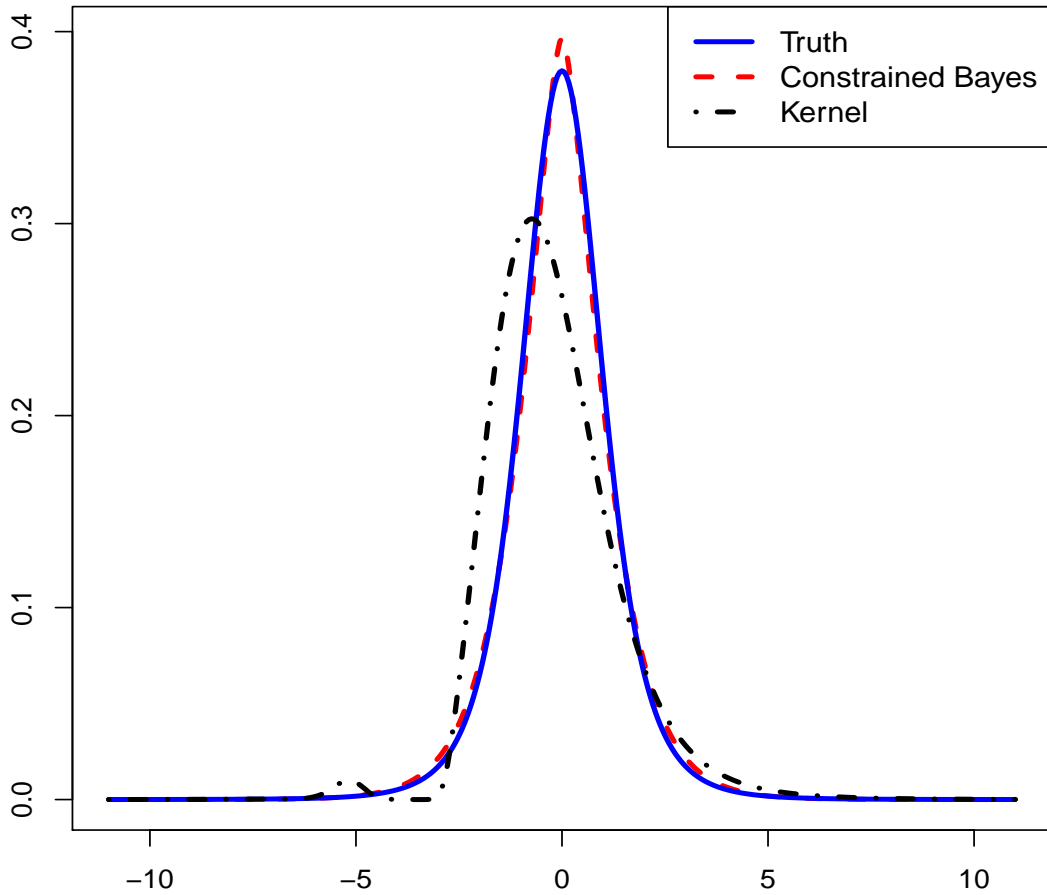


Figure 2: Mean density estimates for the heteroscedastic Normal measurement error simulation of Section 5.2 for sample size $n = 5000$. Solid blue line is the truth (Truth, a t -density with 5 degrees of freedom), the dashed red line is our Constrained Bayes Deconvolution method (Constrained Bayes) and the dash-dotted black line is the deconvoluting kernel density estimator (Kernel).

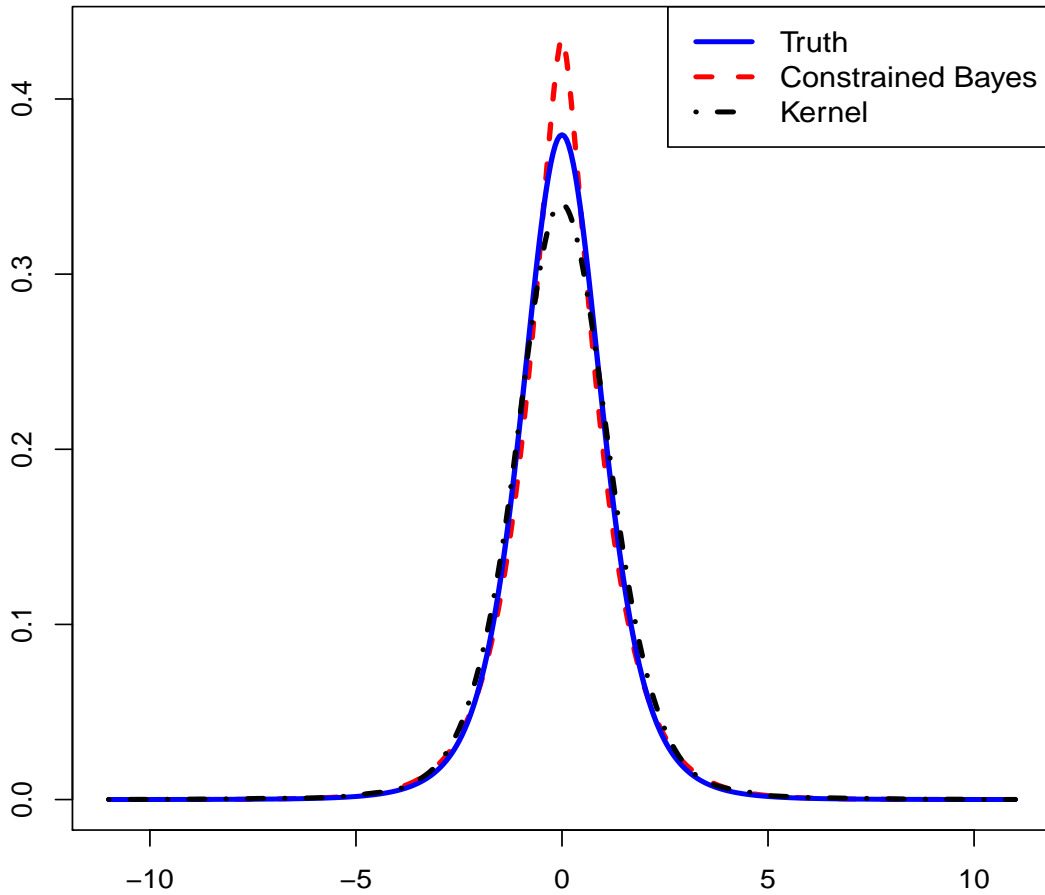


Figure 3: Mean density estimates for the homoscedastic Laplace measurement error simulation of Section 5.2 for sample size $n = 5000$. Solid blue line is the truth (Truth, a t -density with 5 degrees of freedom), the dashed red line is our Constrained Bayes Deconvolution method (Constrained Bayes) and the dash-dotted black line is the deconvoluting kernel density estimator (Kernel).

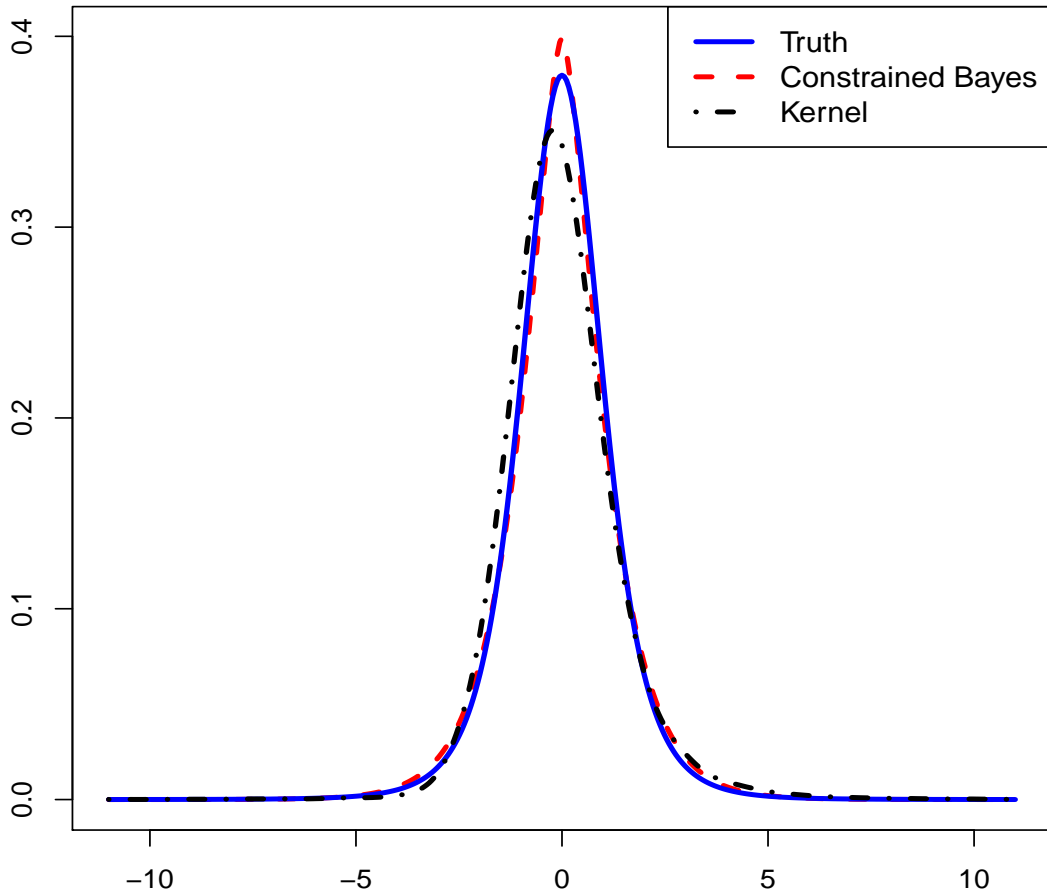


Figure 4: Mean density estimates for the heteroscedastic Laplace measurement error simulation of Section 5.2 for sample size $n = 5000$. Solid blue line is the truth (Truth, a t -density with 5 degrees of freedom), the dashed red line is our Constrained Bayes Deconvolution method (Constrained Bayes) and the dash-dotted black line is the deconvoluting kernel density estimator (Kernel).

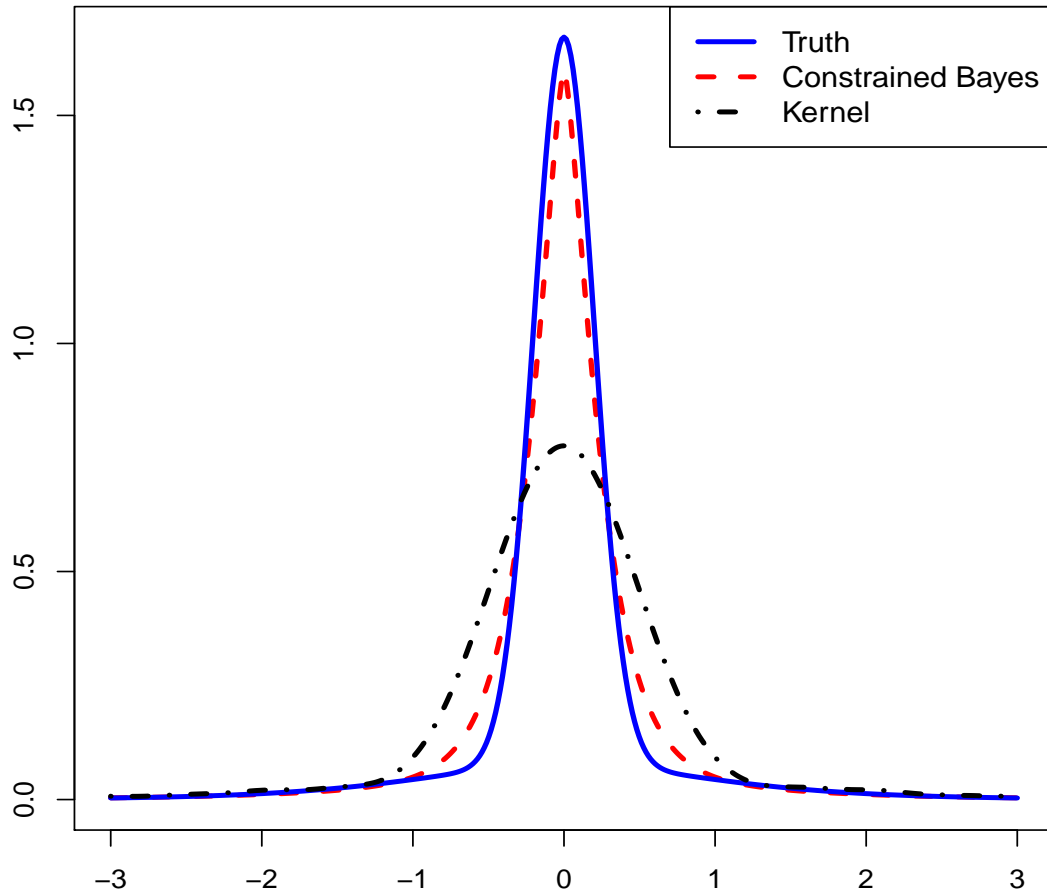


Figure 5: Mean density estimates for the homoscedastic Normal measurement error simulation of Section 5.3 for sample size $n = 5000$. Solid blue line is the truth (Truth, a mixture of a t -density with 5 degrees of freedom and a Normal density with standard deviation 0.2), the dashed red line is our Constrained Bayes Deconvolution method (Constrained Bayes) and the dash-dotted black line is the deconvoluting kernel density estimator (Kernel).

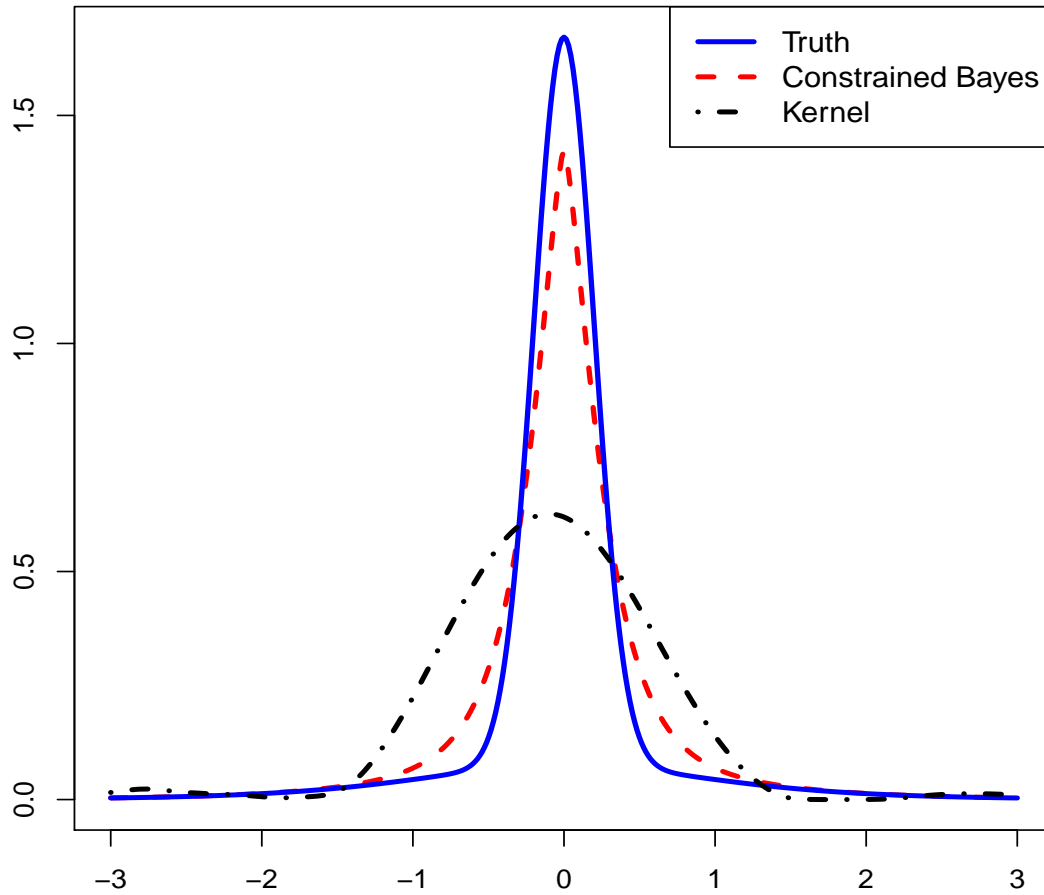


Figure 6: Mean density estimates for the heteroscedastic Normal measurement error simulation of Section 5.3 for sample size $n = 5000$. Solid blue line is the truth (Truth, a mixture of a t -density with 5 degrees of freedom and a Normal density with standard deviation 0.2), the dashed red line is our Constrained Bayes Deconvolution method (Constrained Bayes) and the dash-dotted black line is the deconvoluting kernel density estimator (Kernel).

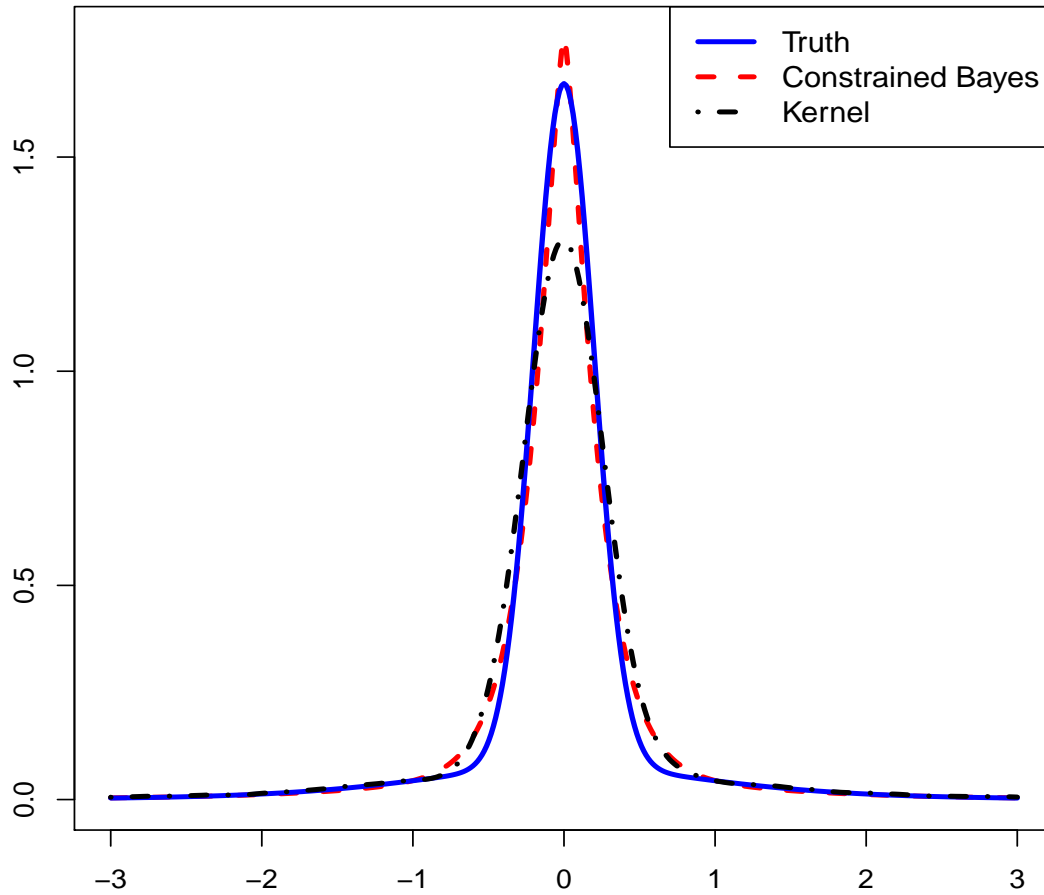


Figure 7: Mean density estimates for the homoscedastic Laplace measurement error simulation of Section 5.3 for sample size $n = 5000$. Solid blue line is the truth (Truth, a mixture of a t -density with 5 degrees of freedom and a Normal density with standard deviation 0.2), the dashed red line is our Constrained Bayes Deconvolution method (Constrained Bayes) and the dash-dotted black line is the deconvoluting kernel density estimator (Kernel).

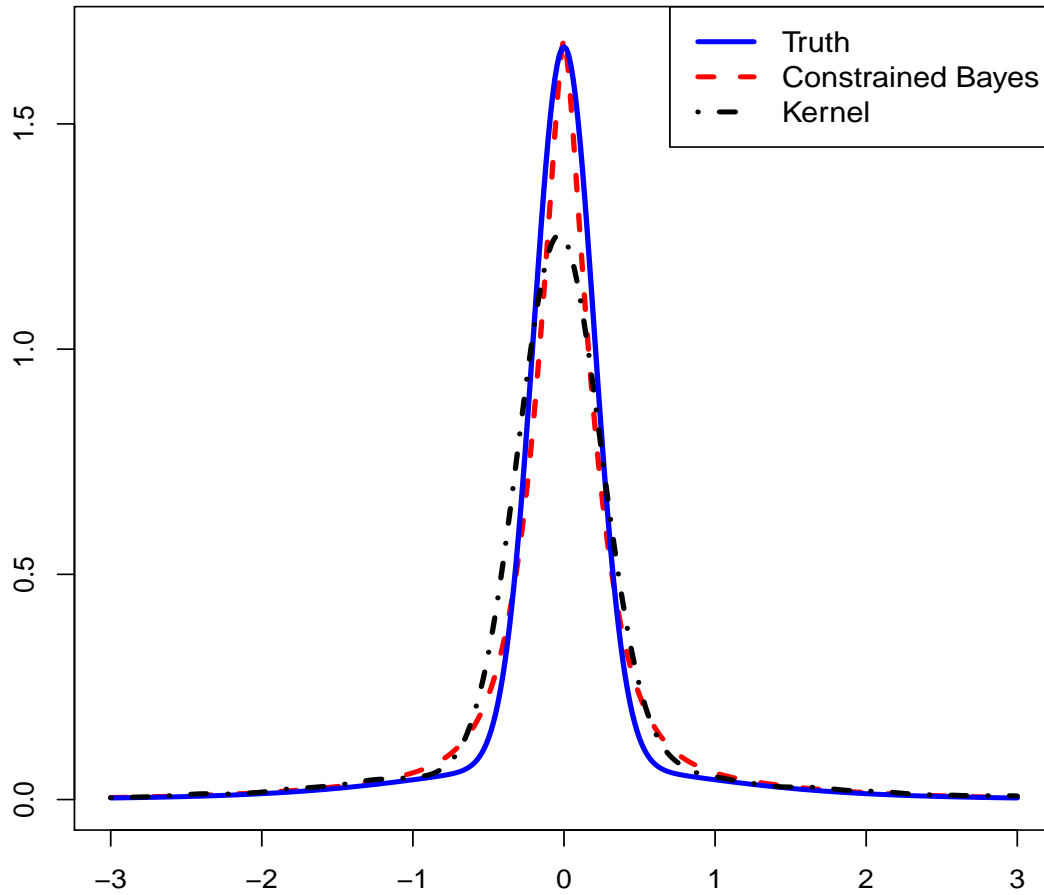


Figure 8: Mean density estimates for the heteroscedastic Laplace measurement error simulation of Section 5.3 for sample size $n = 5000$. Solid blue line is the truth (Truth, a mixture of a t -density with 5 degrees of freedom and a Normal density with standard deviation 0.2), the dashed red line is our Constrained Bayes Deconvolution method (Constrained Bayes) and the dash-dotted black line is the deconvoluting kernel density estimator (Kernel).

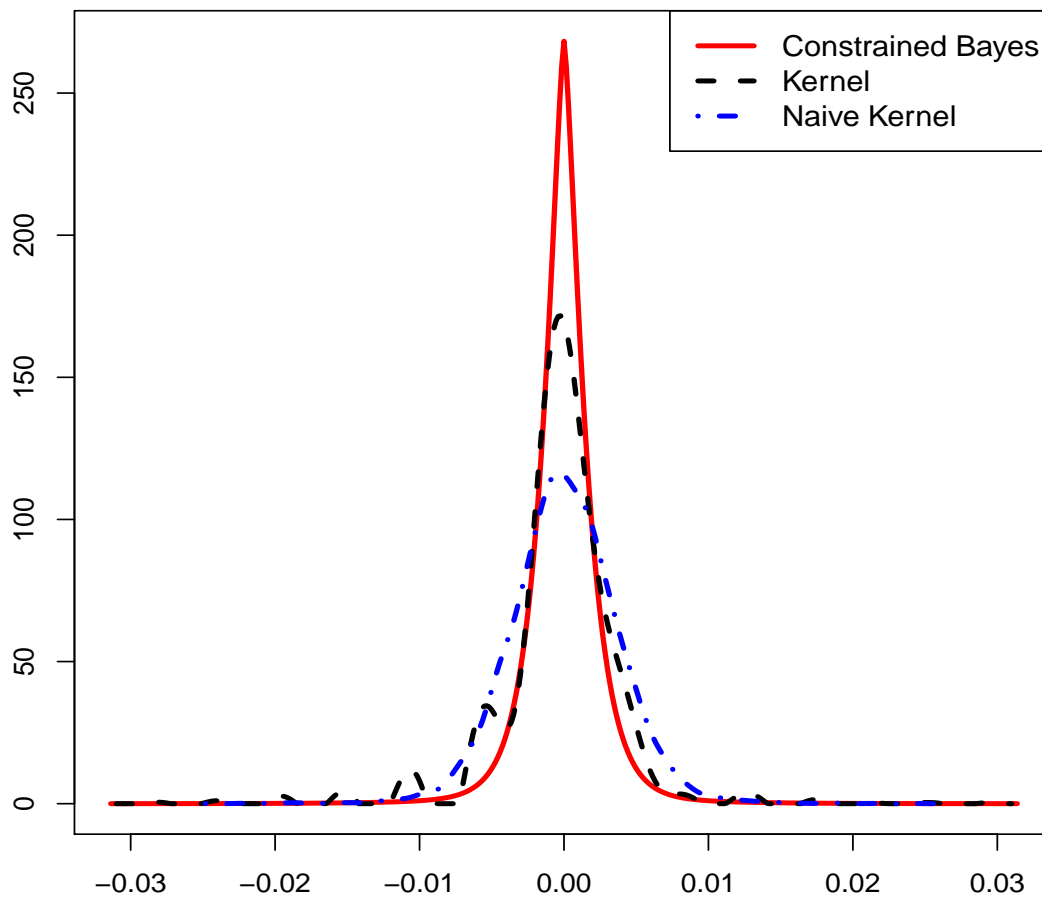


Figure 9: Density estimators for SNP related effect sizes in the GIANT Height data. The solid red line is our Constrained Bayes Deconvolution method (Constrained Bayes), the dashed black line is the deconvoluting kernel density estimator, but the publicly available R programs are too slow to compute this and have memory issue on the full data, so we used a 1% subsample of the data. The dash-dotted blue line is the naive ordinary kernel density estimator ignoring measurement error. The results for the first and third estimators are similar on the same 1% subsample are similar to the full data estimates.

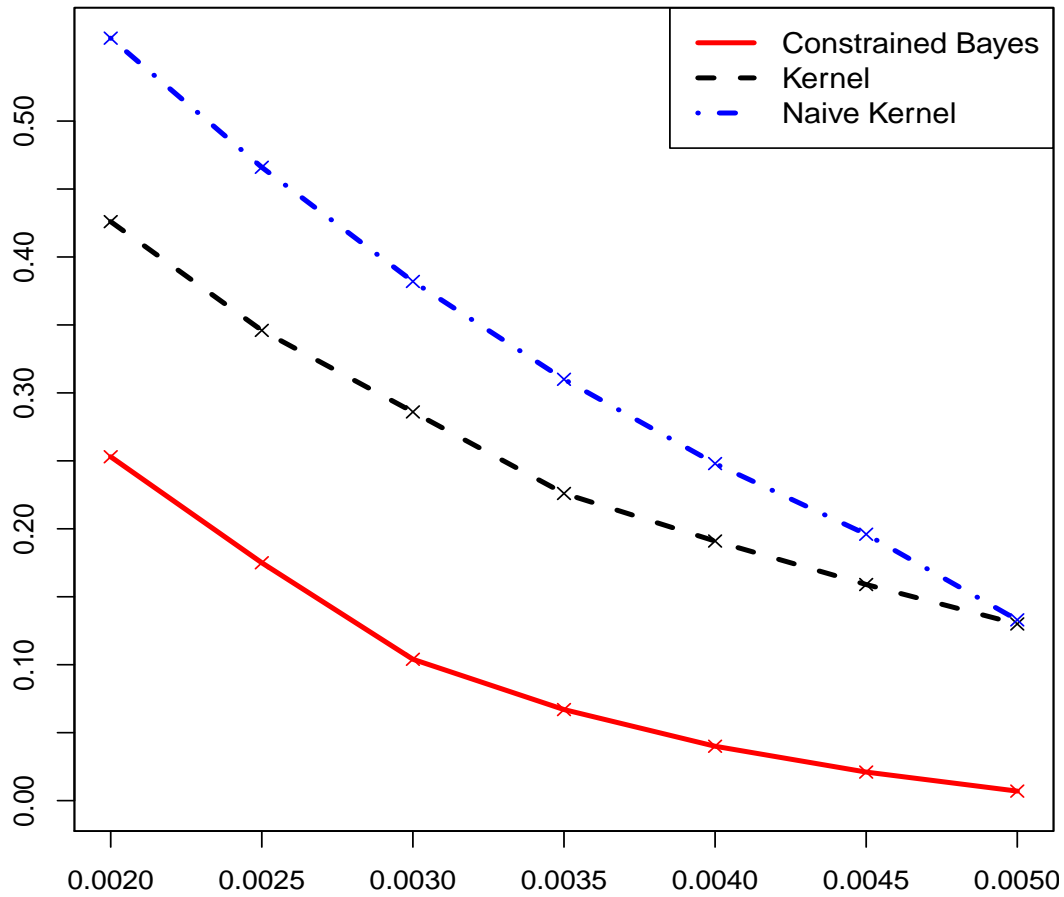


Figure 10: The estimated probability of effect sizes (y-axis) associated with height that the absolute value of effect sizes is greater than the minimum effect size versus the minimum effect size (x-axis) at some discrete choices as in Table 1. The solid red line is based on our Constrained Bayes Deconvolution method (Constrained Bayes), the dashed black line is based on the deconvoluting kernel density estimator (Kernel). The dash-dotted blue line is based on the naive ordinary kernel density estimator (Naive Kernel).

Supplementary Material to *Nonparametric Bayesian Deconvolution of a Symmetric Unimodal Density, with Application to Genomics*

Ya Su

Department of Statistics, University of Kentucky, Lexington, KY 40536-0082, U.S.A.,
ya.su@uky.edu

Anirban Bhattacharya

Department of Statistics, Texas A&M University, College Station, TX 77843-3143, U.S.A.,
anirbanb@stat.tamu.edu

Yan Zhang and Nilanjan Chatterjee

Departments of Biostatistics and Oncology, Johns Hopkins University, Baltimore,
Maryland 21205, U.S.A., yzhan284@jhu.edu and nchatte2@jhu.edu

Raymond J. Carroll

Department of Statistics, Texas A&M University, College Station, TX 77843-3143, U.S.A.
and School of Mathematical and Physical Sciences, University of Technology Sydney,
Broadway NSW 2007, Australia, carroll@stat.tamu.edu

S.1 Overview

In this supplement, we present a microarray example in Section S.1.1 that has the same structure as that of genome wide association studies (GWAS) in Section 6 of the main paper. Section S.1.3 contains some additional simulation results as a complement of the setup in Section 5.3. In addition, we also provide our R code that we used in our analyses. This code uses the RCPP package in R to make our calculations feasible for GWAS.

S.1.1 Microarray Data

The data we use arise from a complicated experimental design, see Davidson et al. (2004). A total of 59 male Sprague-Dawley rats were injected either with saline or the potent carcinogen Azoxymethane (AOM), and then sacrificed. We measured gene expression values for 8,038 genes, log₂ transformed them, and then centered and standardized them. The treatment (AOM versus saline) was then regressed on the gene expressions, resulting in data similar to that of Section 6. There were 4514 genes that had a statistically significant treatment effect with a Bonferroni p-value < 0.05. The effect sizes had a mean of -0.009, a skewness of 0.018 and a kurtosis of 3.56. The variabilities of the regression of treatment on the gene expressions had a minimum of 0.008, a maximum of 0.169, and a 5th percentile of 0.016.

Our Constrained Bayes Deconvolution estimator was applied to the effect sizes associated with treatment. We ran 5000 MCMC iterations under the same hyperparameters used in the simulation sections. We also implemented the rescaled kernel deconvolution estimator in Delaigle and Meister (2008) based on code available at Aurore Delaigle’s web site. In addition, we computed the naive kernel density estimator which ignores measurement error, available in the R package KernSmooth. The results are given in Figure S.1. Here we see the same phenomenon seen in the heteroscedastic simulations (Section 5.2) and the GIANT height data (Section 6.2), namely that the Constrained Bayes estimator recognizes more clearly that many of the effect sizes are small, and hence the density estimate is much more peaked near zero. Another way of writing this is that the kernel methods think there are a more genes with larger effect sizes.

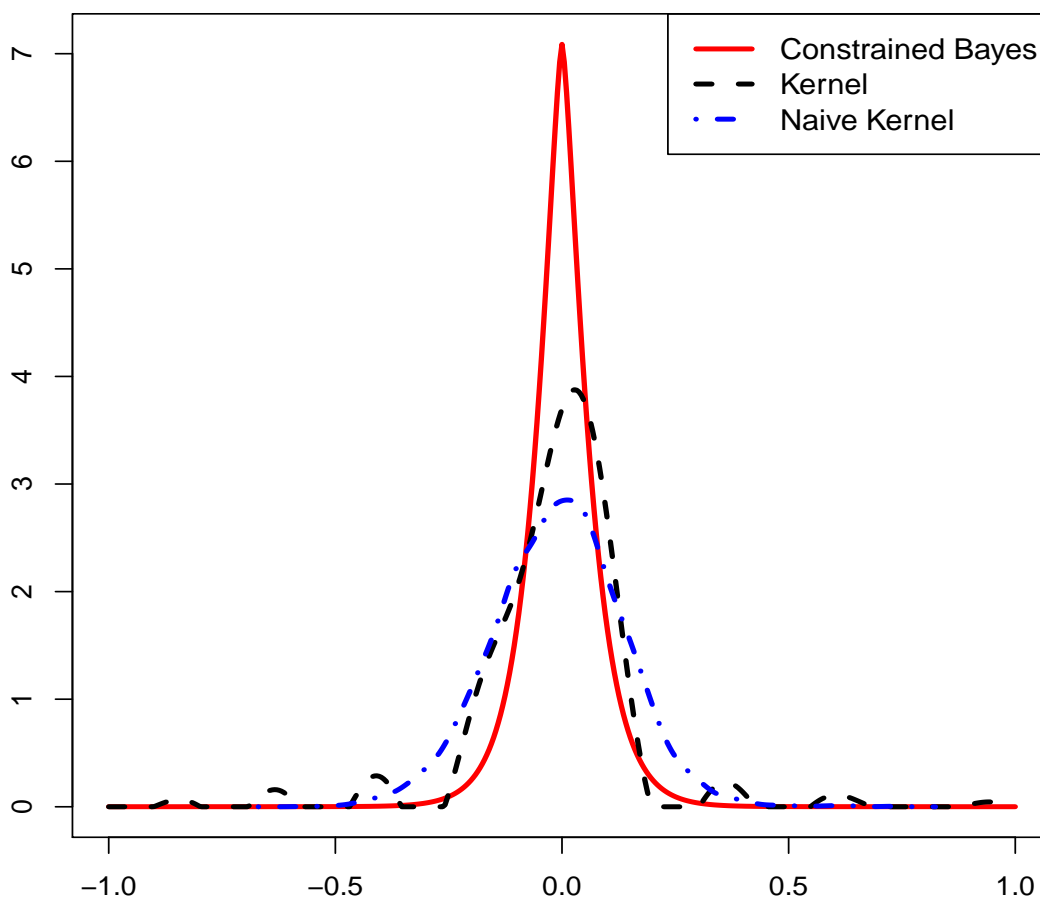


Figure S.1: Density estimators for treatment effect sizes in the microarray data of Section S.1.1. The solid red line is our Constrained Bayesian method (Constrained Bayes). The dashed black line is the deconvoluting kernel density estimator that recognizes measurement error and potential heteroscedasticity. The dash-dotted blue line is the naive ordinary kernel density estimator ignoring measurement error.

Estimator	Minimum effect size					
	0.01	0.05	0.1	0.15	0.2	0.25
Constrained Bayes	0.859	0.425	0.150	0.038	0.000	0.000
Kernel	0.926	0.643	0.357	0.176	0.092	0.067

Table S.2: Comparison of estimated probability of effect sizes associated with treatment that the absolute value of effect sizes is greater than the minimum effect size under our constrained Bayesian method (Constrained Bayes), the deconvoluting kernel density estimator (Kernel) when rats with multiple arrays have their expressions averaged, which ends up with 59 observations.

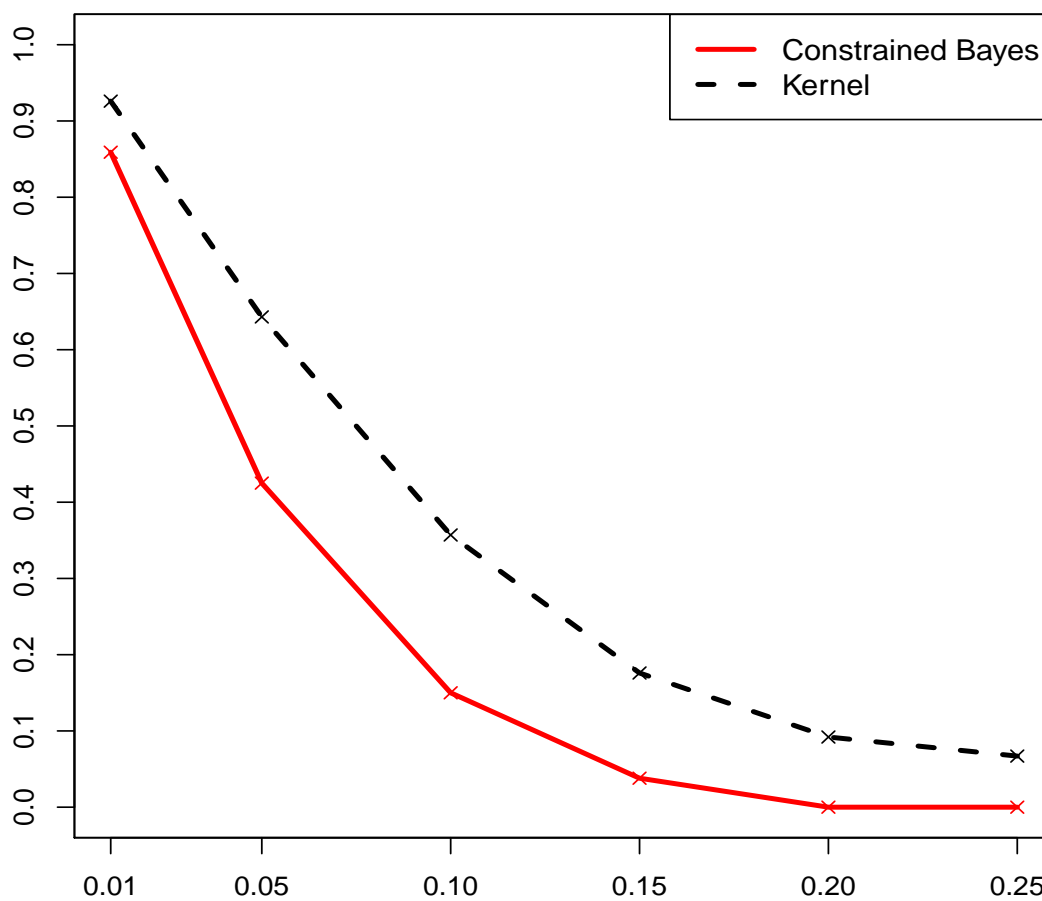


Figure S.2: The estimated probability of effect sizes associated with treatment that the absolute value of effect sizes is greater than the minimum effect size versus the minimum effect size at some discrete choices as in Table S.2. The solid red line is based on our constrained Bayesian method (Constrained Bayes), the dashed black line is based on the deconvoluting kernel density estimator (Kernel).

S.1.2 Details about analysis of GIANT Height data

In this section, we report the procedures for selecting independent SNPs and performing Monte Carlo integration involved in the projection formula, in Section 6.2.

We select a subset of independent SNPs based on linkage disequilibrium (LD) clumping method using PLINK software (Purcell et al., 2007). LD clumping typically sorted SNPs according to the importance (p-values) of SNPs, then took the most significant SNPs and removed SNPs that are correlated with this SNP (squared correlation larger than 0.1) in the window of 1MB base pair distance. Then it went on with the next most significant SNPs that had not been removed yet. Using the data set of Allen et al. (2010), the above LD clumping procedure yields $K = 80349$ independent SNPs.

The projection formula requires an integration with respect to the density of true effect sizes, $f(\beta)$. Since we do not have a closed form for $f(\beta)$, we can borrow information from posterior samples of β_{ij} , the subscripts i and j indicate the effect sizes corresponding to the i th SNP and in the j th MCMC iteration, for $i = 1, \dots, K$, $j = 1, \dots, N$ (K and N represent the total number of SNPs and MCMC iterations). The following steps are performed to complete the calculations for predicting the expected number of significant SNPs:

1. Hypothesize a new sample size n_{new} .
2. To reduce the correlation caused by MCMC chains, we adopt an aggressive thinning at every 50th iteration. For our analysis of Height data, the original MCMC chain contains 50000 iterations (burn-ins excluded), hence $N = 1000$.
3. For any fixed j , compute the expected number of significant SNPs, $\sum_{i=1}^K \text{pow}_{\sigma, \alpha}(\beta_{ij})$, where $\text{pow}_{\sigma, \alpha}(\beta) = 1 - \Phi(z_{\alpha/2} - n_{\text{new}}^{1/2} \sigma^{-1} \beta) + \Phi(-z_{\alpha/2} - n_{\text{new}}^{1/2} \sigma^{-1} \beta)$.
4. Repeat Step 3 for $j = 1, \dots, N$ times. We can obtain posterior samples of the predicted values, and thus, Table 2.

S.1.3 Additional Simulation: The Distribution of X has a Tight Peak Around Zero

We changed the data generating model in Section 5.3 to $\sigma_{00} = 0.1$. Specifically, We implement a mixing of a Normal($0, \sigma_{00}^2$) and a t -distribution with 5 degrees of freedom for the second component, with mixing probabilities 0.8 and 0.2 respectively. We choose the small value $\sigma_{00} = 0.1$ so that the mixing density has a even sharper peak around zero compared to Section 5.3. The additional simulation has only been implemented for normally-distributed error. A similar pattern should be expected when the error distribution is Laplace based on the existing numerical results in Section 5.3.

We first consider a homoscedastic error setup, where $\sigma_i^2 = 0.6^2$ as in Section 5.3. See Figure S.3 for the result of the averaged density over 100 simulations in this setting with $n = 5000$. The numerical comparison for our Constrained Bayes method and the kernel method is given in Table S.3.

n		Constrained	
		Bayes	Kernel
1000	IAE	0.730 (0.041)	1.069 (0.082)
	ISE	1.159 (0.059)	1.068 (0.061)
	Exceedance	0.235 (0.028)	0.415 (0.052)
5000	IAE	0.570 (0.041)	1.018 (0.053)
	ISE	0.916 (0.065)	1.035 (0.040)
	Exceedance	0.147 (0.019)	0.382 (0.030)
10000	IAE	0.508 (0.036)	1.006 (0.047)
	ISE	0.820 (0.061)	1.031 (0.035)
	Exceedance	0.120 (0.015)	0.375 (0.025)
15000	IAE	0.474 (0.046)	0.998 (0.046)
	ISE	0.767 (0.078)	1.023 (0.032)
	Exceedance	0.107 (0.015)	0.369 (0.025)

Table S.3: Comparison of our constrained Bayesian method (Constrained Bayes), the deconvoluting kernel density estimator (Kernel). This is in the first case of Section S.1.3, when the target density is a mixture of t-density with 5 degrees of freedom and a Normal density with standard deviation 0.1, and when the measurement errors are homoscedastic. The sample size is n , IAE is integrated absolute error, ISE is integrated squared error and Exceedance is the absolute difference between the exceedance probability under the estimated density and that under the true density. Numbers in parentheses are standard errors.

We implement the heteroscedastic and select σ_i^2 as in Section 5.3, specifically, $\sigma_i^2 = (0.75 + X_i/4)^2$. Figure S.4 shows the estimated density averaged over 100 simulated data sets with $n = 5000$. The numerical comparison for our Constrained Bayes method and the kernel method is given in Table S.4.

n		Constrained	
		Bayes	Kernel
1000	IAE	0.847 (0.053)	1.175 (0.033)
	ISE	1.307 (0.063)	1.138 (0.021)
	Exceedance	0.311 (0.033)	0.497 (0.026)
5000	IAE	0.668 (0.044)	1.159 (0.016)
	ISE	1.067 (0.062)	1.126 (0.010)
	Exceedance	0.216 (0.023)	0.480 (0.012)
10000	IAE	0.578 (0.040)	1.154 (0.015)
	ISE	0.935 (0.061)	1.123 (0.008)
	Exceedance	0.177 (0.018)	0.473 (0.010)
15000	IAE	0.532 (0.045)	1.149 (0.012)
	ISE	0.862 (0.074)	1.119 (0.006)
	Exceedance	0.159 (0.017)	0.469 (0.009)

Table S.4: Comparison of our constrained Bayesian method (Constrained Bayes), the deconvoluting kernel density estimator (Kernel). This is in the second case of Section S.1.3, when the target density is a mixture of t-density with 5 degrees of freedom and a Normal density with standard deviation 0.1, and when the measurement errors are heteroscedastic. The sample size is n , IAE is integrated absolute error, ISE is integrated squared error and Exceedance is the absolute difference between the exceedance probability under the estimated density and that under the true density. Numbers in parentheses are standard errors.

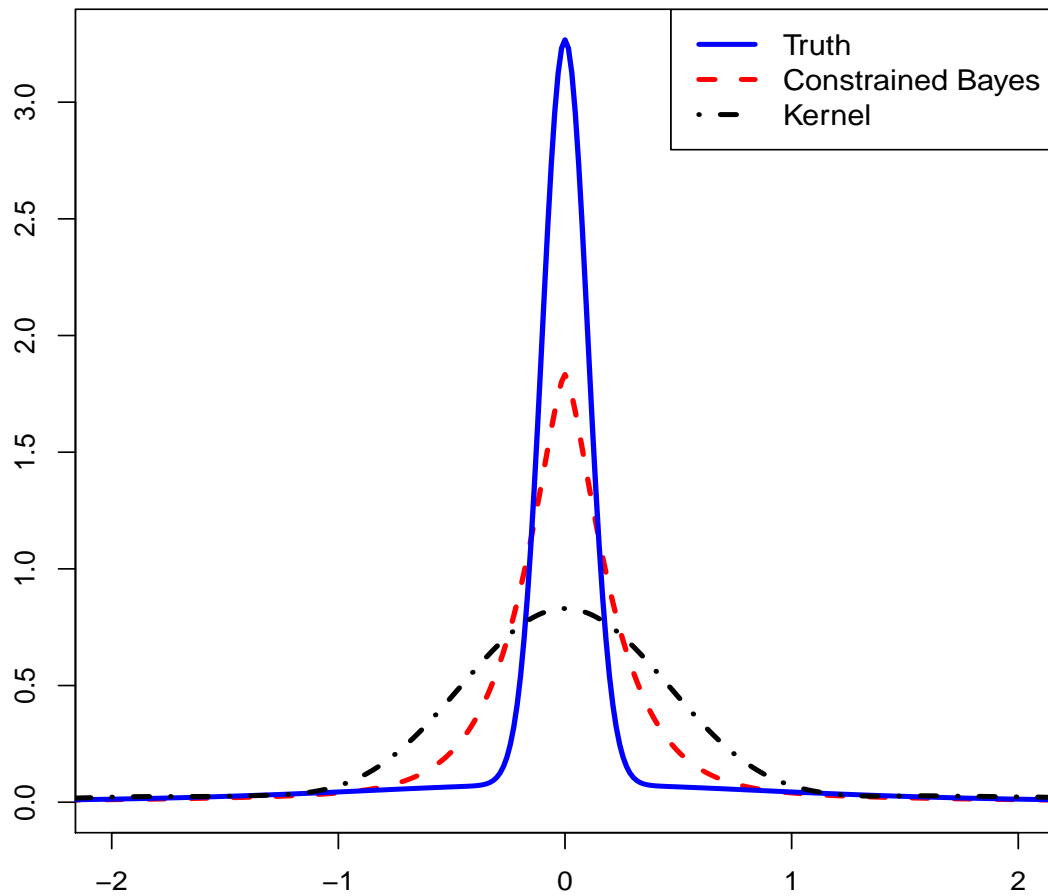


Figure S.3: Mean density estimates for the homoscedastic simulation of Section S.1.3 for sample size $n = 5000$. Solid blue line is the truth (Truth, a mixture of a t -density with 5 degrees of freedom and a Normal density with standard deviation 0.1), the dashed red line is our constrained Bayesian method (Constrained Bayes) and the dash-dotted black line is the deconvoluting kernel density estimator (Kernel).

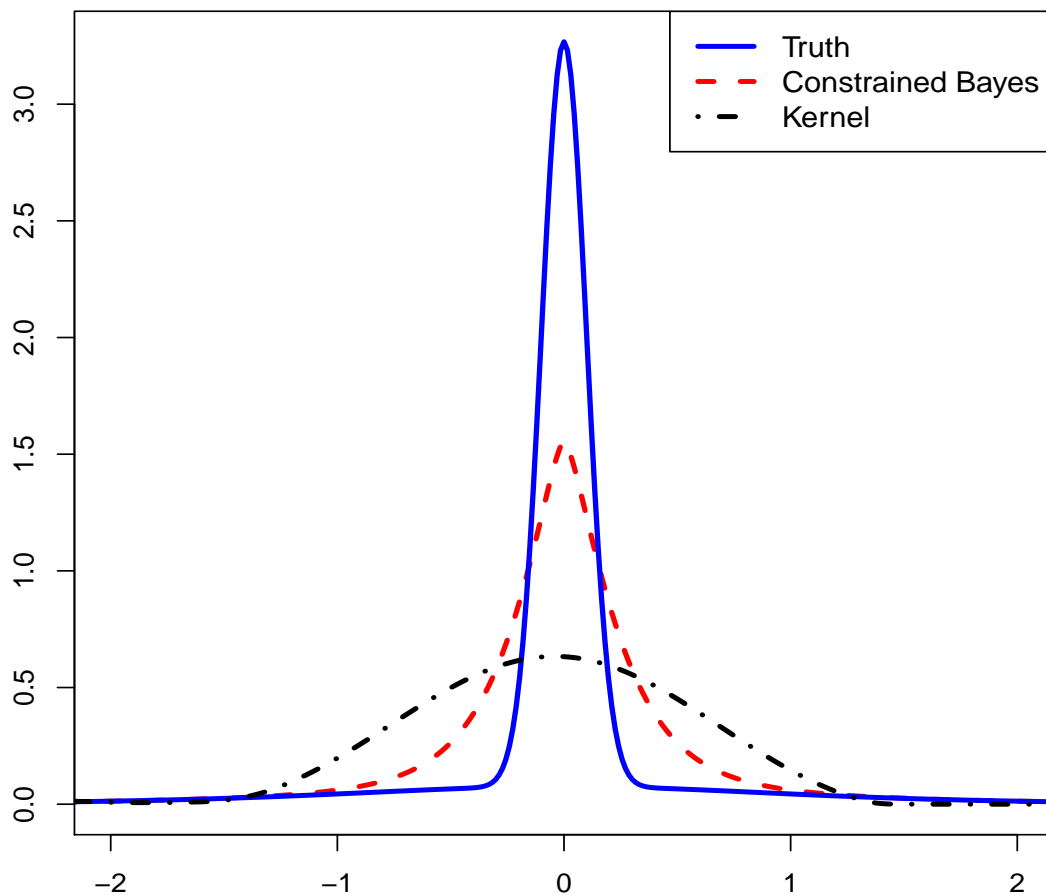


Figure S.4: Mean density estimates for the heteroscedastic simulation of Section S.1.3 for sample size $n = 5000$. Solid blue line is the truth (Truth, a mixture of a t -density with 5 degrees of freedom and a Normal density with standard deviation 0.1), the dashed red line is our constrained Bayesian method (Constrained Bayes) and the dash-dotted black line is the deconvoluting kernel density estimator (Kernel).